APPLICATIONS OF NORMAL MODE ANALYSIS TO OCEAN ACOUSTIC TOMOGRAPHY

by

JOSEPH JACOB ROMM
B. S. PHYSICS, M.I.T
(1982)

SUBMITTED TO THE DEPARTMENT OF PHYSICS
IN PARTIAL FULFILLMENT OF THE REQUIREMENTS
FOR THE DEGREE OF

DOCTOR OF PHILOSOPHY

at the

MASSACHUSETTS INSTITUTE OF TECHNOLOGY
March 1987

Signature of Author Signature redacted
Department of Physics
March, 1987

Certified by Signature redacted
Kosta Tsipis
Thesis Supervisor

Accepted by Signature redacted
George Koster
Chairman, Department Committee

to

Ethel Grodzins Romm,

the finest person I know, by far

Table of Contents

ACKNOWLEDGMENTS

I would not have become a physicist were it not for Lee Grodzins. He stands in my mind as the model physicist.

Kosta Tsipis made it possible for me to find my niche in physics. His passion for the truth and his unfailing confidence in me have been my two great lights during the past five years.

Walter Munk found me the perfect thesis, for which I am permanently in his debt. I hope some day to be as open-minded as he is.

Guy Masters' willingness to both share his work with me and put up with my constant interruptions made this thesis possible. Peter Worcester was always available for advice. It is difficult for me to imagine two more tireless or competent scientists.

Bruce Howe and Bruce Cornuelle's knowledge and guidance proved invaluable to my work.

I thank Dave Horwitt, Betty Ma, and Flicki Dormer for sharing with me a portion of their computer expertise.

Don Betts did his usual outstanding job on my figures.

I am grateful to many people who helped me feel at home at IGPP: Bob Truesdale, Doug Peckham, Steve Abbot, Jane DiTullio, Mary Jones, and Bob Knox. Special thanks go to Kevin Hardy for convincing me to buy a MacIntosh, which greatly simplified the writing of this thesis.

I thank my committee for helping me to strengthen this thesis.

Throughout my work I was funded by the Program in Science and Technology for International Security.

APPLICATIONS OF NORMAL MODE ANALYSIS TO OCEAN ACOUSTIC TOMOGRAPHY

by

JOSEPH JACOB ROMM

Submitted to the Department of Physics on March 20, 1987
in partial fulfillment of the requirements for the Degree of
Doctor of Philosophy in Physics

ABSTRACT

The rapid means of calculating normal modes in a waveguide developed in seismology have been applied to ocean acoustics. A comparison of mode theory with WKBJ and ray theory in the mid-latitudes was made. Here, a comparison was also made with precise measurements of the impulse response of the ocean sound channel made during the 1983 Reciprocal Acoustic Transmission Experiment at 300-km range, with source and receiver near the sound channel. Both ray theory and WKBJ theory were found to be adequate techniques for predicting the acoustic arrival pattern at 400 Hz in this geometry for the range-averaged ocean. Adiabatic normal mode theory proved adequate to account for the effects of the variation of the vertical sound speed profile with range.

Normal mode theory was shown to be better suited than WKBJ theory for monitoring changes in the top 500 meters of the Greenland Sea water column at 250 Hz and 300 km range. Normal mode travel times (group velocities) were used to constrain sound speed. The possibility of achieving high precision -- ±0.05 m/s or ±0.01 degrees C -- for the range averaged ocean was demonstrated (although a formal resolution analysis must still be done). A technique for isolating individual modes from the acoustic waveforms observed at a variety of receiver depths was developed. Computations carried out with this mode filtering technique suggest that, for an upcoming Greenland Sea tomography experiment, a relatively shallow source (150 m) and a vertical array of receivers with a 30 to 50 m spacing and a shallow receiver near 50 m seems optimum. The effect of a smooth ice layer on sound propagation in the Greenland Sea was examined and found to be insignificant for ice layers under 5 meters thick.

Thesis Supervisor: Dr. Kosta Tsipis

1. INTRODUCTION

Because the ocean is a naturally occurring waveguide, sound propagation through it can be described as a sum of normal modes. The normal mode calculation is more exact, though more time-consuming, than approximations such as geometric ray optics or WKBJ theory. This thesis will describe the theory, implementation, and applications of a rapid means of calculating normal mode propagation.

In the mid-latitudes, there is a sound speed minimum near a depth of 1000 meters, with sound speed increasing above this axis because of increasing temperature, and below this axis because of increasing pressure. In the language of geometric ray optics, the oceanic waveguide acts like a lens, constantly refracting sound toward the sound channel axis. This lens has a focal length of about 25 kilometers and, in the case of long-range sound transmission, gives rise to quasisinusoidal acoustic ray paths connecting source and receiver.

In the Greenland Sea, the temperature is relatively constant below 200 meters and so sound speed increases fairly uniformly with depth. In this waveguide, sound is constantly bent toward

the surface, and then reflected off the air-water interface. If the sound speed increases linearly with depth, the rays are arcs of circles connected at the surface.

Analysis of underwater acoustic signals as a sum over normal modes has been used since Pekeris [*1948*]. In horizontally stratified media like the oceans, normal modes involve Hankel functions in the range, and non-analytical functions with depth.

Although the modal approach to acoustic propagation is not as easy to visualize as ray descriptions, it handles diffraction and focal points where ray approximations break down. The chief impediment to its use has been the relative difficulty in quickly calculating the large number of normal modes that are required to represent propagation over long ranges in the deep ocean. For this reason, ray and WKBJ theory have been the primary means of calculating long-range, synthetic acoustic arrival patterns in the ocean.

Yet the theory of rapid means of calculating modes has existed in the seismological literature since Haskell [*1953*]. The computational algorithms described by Woodhouse [*1980*], and applied to a synthetic seismogram program by Masters, is here applied to propagation of sound in the ocean.

The specific applications in this thesis are related to a technique for mapping large-scale ocean features called ocean acoustic tomography. Developed over the past 10 years [*Munk and Wunsch, 1979*], ocean tomography makes use of the fact that as

sound travels though the ocean, it picks up information about the sound speed and current velocity of the water it passes through. Since different acoustic ray paths sample different parts of the ocean, the arrival time of these rays can be used to infer a depth- and range-dependent picture of the ocean's structure, using geophysical inverse techniques.

The present motivation for using tomography is the study of mesoscale disturbances, "ocean weather" that accounts for perhaps 99% of the kinetic energy of the ocean circulation -- the other 1% being the general circulation, or "climate," of the ocean [*Munk and Wunsch, 1979*]. Because tomography allows the study of water masses extending over hundreds of kilometers for months at a time, it is well suited for examining the ocean mesoscale.

The first application of normal modes to be considered in this thesis is the comparison of mode theory with WKBJ and ray theory in the mid-latitudes. Here, a comparison will also be made with precise measurements of the impulse response of the ocean sound channel made near Bermuda during the 1983 Reciprocal Acoustic Transmission Experiment (RTE83) at 300-km range, with source and receiver near the sound channel.

Tomographic inverse procedures allowed range-dependent information to be deduced from the data [*Howe, 1986*]; that is, sound speed as a function of depth and range was determined. To account for the effects of range-dependence in normal mode theory, adiabatic mode theory was used. This theory has been

developed for use in long-range underwater propagation since Pierce [*1965*].

The second application of normal mode theory examined in this thesis is sound propagation in the Greenland Sea. The Greenland Sea has been of particular interest since it was discovered that it may be one of the driving forces behind deep-ocean circulation. Here, mode theory will be compared with WKBJ theory for a variety of measured range-independent profiles. To model sound propagation in the winter, the effect of an ice layer on top of the ocean will be examined.

WKBJ theory is inadequate to describe the entire acoustic arrival pattern in the Greenland Sea [*Topuz and Felsen, 1985*]; it cannot be used in the tomographic inverse to provide an accurate estimate of the vertical sound speed profile near the surface. For this reason, the usefulness of normal modes for tomographic inversion will be examined. I will examine inversions based on group velocities, that is, on modal arrival times. I will also describe how a vertical array of acoustic receivers can be used as a mode "filter" to isolate individual modes from the observed acoustic waveforms. I will try to determine whether or not modal inversions can yield significant information about the vertical sound-speed profile that ray inversions cannot.

The structure of this thesis is as follows. In Chapter Two, I give the theory of normal mode propagation in the ocean and discuss the technique for rapidly calculating the acoustic arrival

patterns. This chapter will also treat range-dependent adiabatic normal mode theory, the theory of sound propagation in the presence of an ice layer, the basics of tomographic inverse theory, and the theory of the mode filter.

Readers interested primarily in the results of applying this normal mode treatment to long-range underwater acoustics should skip Chapter Two and go directly to Chapter Three, which discusses the RTE83 experiment, and the application of range-independent and adiabatic theory to it. Chapter Four deals with the Greenland Sea, comparing the results of WKBJ theory and normal mode theory. The effects of an ice layer on modal propagation is examined. Finally, in Chapter Five, modal inversions are studied. Chapter Six presents discussion and conclusions. The Appendices detail some of the computational methods involved in the calculations.

2. THEORY

Normal modes in the ocean are a solution to the acoustic wave equation for a laterally homogeneous, vertically heterogeneous ocean.

The coordinate system used here is shown in Figure 2.1. The air-water interface is at z=0 and the z-axis is taken as positive downwards. The r-axis lies in the direction of the line connecting the acoustic source and the receiver.

It is the assumption of a laterally homogeneous ocean that makes cylindrical coordinates most convenvient. This assumption means that only sound propagating in the r-z plane need be considered. For the kind of long-range propagation examined here, Munk [*1980*] has shown that it is reasonable to neglect sound that travels out of this plane and is then refracted back into the plane.

The acoustic equation is derived from linearizing the equations of motion.

2.1 The Acoustic Forward Problem

Newton's Second Law for a perfectly elastic (non-viscous), isotropic fluid element is

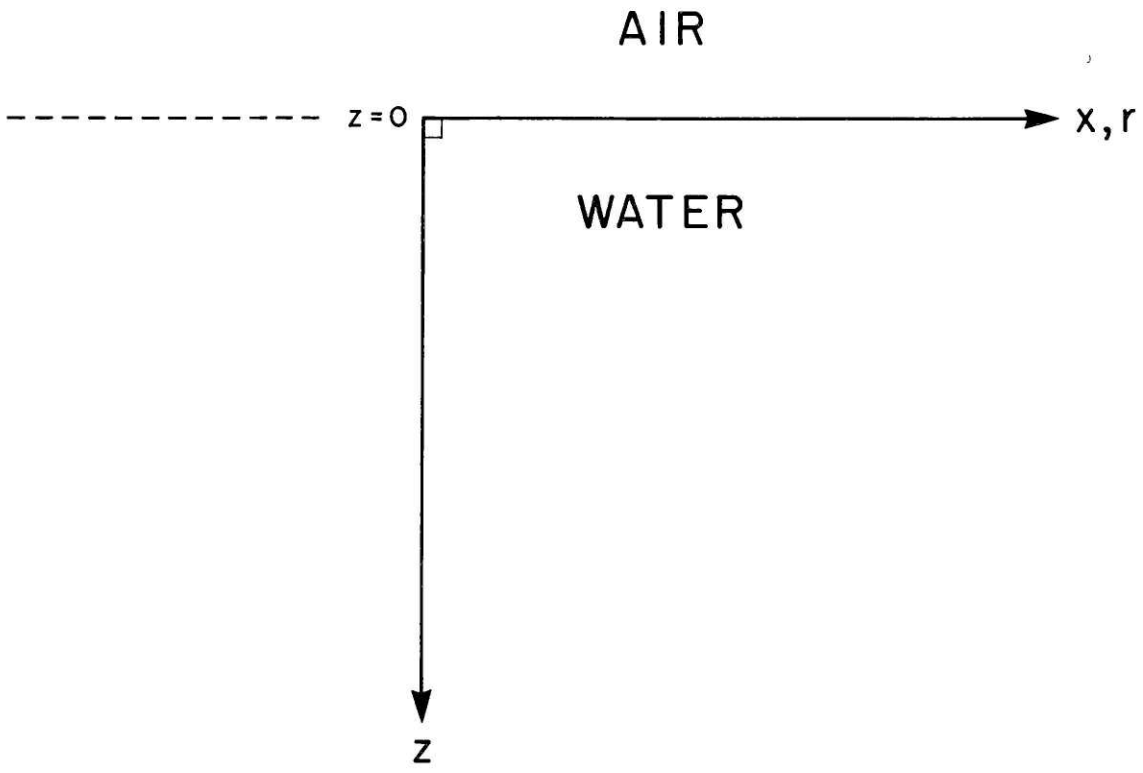

Figure 2.1. The air-water coordinate system used for acoustic normal mode propagation.

$$\tilde{\rho}(\partial\tilde{\mathbf{u}}/\partial t + \tilde{\mathbf{u}}\cdot\nabla\tilde{\mathbf{u}}) = -\nabla\tilde{p} + \tilde{\rho}\mathbf{g} - Q\cdot\tilde{\mathbf{u}} \qquad \text{T.1}$$

where $\tilde{\rho}$ is the density

$\tilde{\mathbf{u}}$ is the velocity field

$\tilde{p}$ is the pressure

$\mathbf{g}$ is the gravity field

Q is the rate of creation of mass per unit volume in the element. It is used to model the acoustic source

$\partial\tilde{\mathbf{u}}/\partial t$ is the local rate of change of $\tilde{\mathbf{u}}$ at a fixed point.

$\tilde{\mathbf{u}}\cdot\nabla\tilde{\mathbf{u}}$ is how the fluid element's velocity changes owing to its changing position in space.

The equation of continuity (conservation of mass) for a fluid is

$$\partial\tilde{\rho}/\partial t + \tilde{\mathbf{u}}\cdot\nabla\tilde{\rho} + \tilde{\rho}\cdot\nabla\tilde{\mathbf{u}} = Q \qquad \text{T.2}$$

In the absence of an acoustic wave ($Q=0$), the fluid variables have the time-independent values,

$\tilde{\rho} = \rho_0$

$\tilde{p} = p_0$

$\tilde{\mathbf{u}} = \mathbf{u}_0 = 0$ (the fluid is stationary).

With these values, the solution to T.1 is

$$\nabla p_0 = \rho_0 \mathbf{g}$$

To examine the effect on the fluid of a small perturbation, such as an acoustic wave, the following representation is used:

$$\tilde{\rho} = \rho_0 + \rho$$
$$\tilde{p} = p_0 + p$$
$$\tilde{\mathbf{u}} = \mathbf{u}_0 + \mathbf{u} = \mathbf{u}$$

In linear theory, the disturbances -- ρ, p, $\mathbf{u}$ (and Q) -- are so weak that in the equations of motion they are treated as small quantities whose products are neglected; for example, in equation T.1, the second term in the parenthesis is neglected, as is the $Q \cdot \tilde{\mathbf{u}}$ term. In the perturbation expansion of T.2, terms like $\mathbf{u} \cdot \nabla \rho$ and $\rho \cdot \nabla \mathbf{u}$ are, similarly, the products of small quantities.

The effect of gravity will be neglected, which is equivalent to assuming that $\partial \rho_0 / \partial z = 0$ -- the density is independent of depth. This is a good assumption, except at very low frequencies, below one Hertz, where the wavelength of sound is very large [*Boyles, 1984*]. (This term can be neglected whenever the wavelength of sound is much smaller than the vertical scale of variation in density. At the frequencies considered here, the wavelength of sound is under 10 meters, while the total change of water density with depth in the ocean is limited to about 4%, found at 10 km.)

This leaves the linearized equation of motion

$$\rho_0 \cdot \partial \mathbf{u}/\partial t = -\nabla p \qquad \text{T.3}$$

Linearizing equation T.2 means neglecting the second term (the product of small quantities). Defining the Compressibility, κ, for a volume of fluid, V, held at constant entropy, S, as

$$\kappa = -(1/V)(\partial V/\partial p)_S = (1/\rho_0)(\partial \rho/\partial p)_S$$

allows the continuity equation to be written as

$$\kappa \cdot \rho_0 \cdot \partial p/\partial t = -\rho_0 \cdot \nabla \cdot \mathbf{u} + Q \qquad \text{T.4}$$

Taking the divergence of T.3 (neglecting $\partial \rho_0/\partial z$ again) and substituting T.4 yields the acoustic wave equation:

$$\nabla^2 p - (1/\alpha^2)(\partial^2 p/\partial t^2) = -\partial Q/\partial t$$

where the speed of sound, α, is thereby defined as $\alpha = \sqrt{1/\kappa\rho_0}$

[For a plane wave p, both ∇p and $(1/\alpha)\cdot(\partial p/\partial t)$ are of the order of $k=\omega/\alpha=2\pi/\lambda>1/(2m)$ at the frequencies of interest. Terms like $(1/\rho_0)\cdot(\partial \rho_0/\partial z)\approx 1/(200km)$ and $(\nabla p_0)/(\rho_0 \cdot c^2)=g/c^2\approx 1/(200km)$ are very much smaller, which is why they have been neglected.]

Thus, the wave that propagates through the ocean is a balance

between the restoring force -- the elasticity, $1/\kappa$, that causes the water to tend to return to its original uncompressed state -- and the inertia -- which is proportional to the mass density, ρ_0.

The speed of sound in the ocean varies with pressure, temperature, and salinity. Sound speed increases with pressure, and therefore with depth, about 6 m/s for every 100 m depth increase. Sound speed increases about 5 m/s for each increase in temperature of one Centigrade degree. Sound speed increases about 1.3 m/s for each part per thousand increase in salinity. Over most of the ocean, the vertical variation of salinity is not large enough to have much effect on the speed of sound [*Boyles, 1984*].

In the mid-latitudes, a waveguide exists around the sound speed minimum at about 1 km because above 1 km, the increase in temperature increases sound speed (more than the decrease in pressure decreases it), whereas below 1 km, the increase in pressure increases sound speed (while the decrease in temperature becomes negligible).

In the Greenland Sea, the vertical temperature is far more uniform, and the waveguide is created primarily by the effect of pressure, which creates a nearly linear increase in sound speed with depth.

The existence of a waveguide means that sound propagation can be described as a sum of normal modes, and the symmetry suggests that the wave equation be solved by means of separation

of variables.

Now, consider an isotropic source whose sinusoidally varying radius is much less than a wavelength, described by a source radiating in three dimensions

$$\partial Q/\partial t = A \cdot \delta(\mathbf{r}-\mathbf{r}_s)e^{-i\omega t}$$

where $\delta(\mathbf{r}-\mathbf{r}_s)$ is the Dirac delta function

$\mathbf{r}_s$ is the position vector of the source

ω is the angular frequency of the source

A is an amplitude factor

A single frequency source suggests a single frequency solution. Following Boyles [*1984*], to separate time from the spatial variables, let

$$P(\mathbf{r},t) = p(\mathbf{r})e^{-i\omega t}$$

where the sound pressure amplitude, $p(\mathbf{r})$, is time independent.

Substituting into the acoustic equation, and assuming a unit amplitude source for convenience

$$\nabla^2 P - (1/\alpha^2)(\partial^2 P/\partial t^2) = - \delta(\mathbf{r}-\mathbf{r}_s)e^{-i\omega t}$$

yields for $p(\mathbf{r})$ the Helmholtz equation

$$\nabla^2 p + \gamma^2 p = -\delta(r-r_s)$$

where the wavenumber, γ, has been defined as $\gamma=\omega/\alpha$.

The assumption of cylindrical symmetry discussed at the beginning of this section reduces the problem to two dimensions, and yields a new form for the equation in cylindrical coordinates (the Earth's sphericity is taken into account by means of the Earth flattening transformation of Muller [*1970*] and Chapman [*1973*]):

$$\partial^2 p/\partial r^2 + (1/r)(\partial p/\partial r) + \partial^2 p/\partial z^2 + \gamma^2 p = -(1/2\pi r)\delta(r)\delta(z-z_s) \qquad T.5$$

2.2 The Normal Mode Solution

Consider a horizontally stratified ocean, $\alpha=\alpha(z)$, $\gamma=\gamma(z)$, in the form of a waveguide that locks the source's acoustic energy into the ocean. The solution may be described as an outgoing wave from the source in the form

$$p(r,z) \doteq H_0^{(1)}(kr)Z(z,k)$$

where $H_0^{(1)}(kr)$ is the horizontal wavefunction

k will be identified with the horizontal wave number

Z(z,k) is the vertical wavefunction, satisfying the equation

$$d^2Z/dz^2 + [\gamma^2(z) - k^2]\cdot Z = 0 \qquad T.6$$

$H_0^{(1)}(kr)$ is the zero-order Hankel function of the first kind, whose asymptotic form for large r ($kr >> 1$) shows the characteristic $r^{-1/2}$ decay:

$$H_0^{(1)}(kr) \approx (2/kr)^{1/2} \cdot e^{i(kr-\pi/4)}$$

Boundary conditions on the top and bottom of the ocean are required to solve equation T.6. A free-surface condition, in which the pressure at the surface $Z(z=0)$ vanishes, is used here. This would be an exact condition if the surface of the water were at a vacuum, but it is still a very good approximation for air: Even for sound normally incident on the air-water interface from the water side, only one part in a thousand of the acoustic energy is transmitted into the air; the rest is reflected back into the water [*Brekhovskikh and Lysanov, 1982*]. The bottom condition used here is that all the energy is locked in the ocean by forcing both Z and dZ/dz to vanish as $z \rightarrow \infty$. This approximation neglects the so-called "leaky modes" that continuously radiate into the bottom of the ocean. (A partially reflecting bottom, while more realistic, was not used because it was considered an unnecessary complication for the kind of acoustic propagation considered here. At a frequency of a few hundred Hertz, sound is severely attenuated each time it is reflected from the bottom, by as much as a factor of 10 --10dBs -- or more. This leads to rapid

attenuation of bottom-interacting acoustic waves for sound propagating over hundreds of kilometers [*Brekhovskikh and Lysanov, 1982*].)

These boundary conditions lead to a characteristic equation for $Z(z,k)$ with eigenvalues k_n and eigenfunctions $Z(z,k_n)$, which implies that the solution of the inhomogeneous equation can be written as a sum of normal modes:

$$P(r,z) = \sum_n A_n \cdot H_0^{(1)}(k_n r) \cdot Z_n(z)$$

where $Z_n(z) \equiv Z(z,k_n)$. A_n is a constant to be determined.

To demonstrate that this is a solution of the Helmholtz equation, and to find A_n, substitute it in T.5 and make use of T.6 and the relation [*Brekhovskikh and Lysanov, 1982*]

$$(d^2/dr^2 + r^{-1}d/dr + k_l^2)H_0^{(1)}(k_l r) = (2i/\pi r)\delta(r)$$

which yields

$$\sum_n A_n \cdot Z_n(z) = (i/4)\delta(z-z_s)$$

Multiplying by $Z_m(z)$, and integrating over z, gives

$$\int \sum_n A_n \cdot Z_n(z) \cdot Z_m(z) dz = \int (i/4)\delta(z-z_s) Z_m(z) dz$$

where the integrals extend over the entire ocean.

Making use of the orthogonality of the eigenfunctions and normalizing them such that

$$\int \sum_n Z_n(z) \cdot Z_m(z) dz = \delta_{nm}$$

yields

$$\sum_n A_n \cdot \delta_{nm} = (i/4) Z(z_s)$$

$$\Rightarrow \quad A_m = (i/4) \cdot Z(z_s)$$

$$\Rightarrow \quad P(r,z) = (i/4) \cdot \sum_n H_0^{(1)}(k_n r) \cdot Z_n(z_s) \cdot Z_n(z) \qquad \text{T.7}$$

To solve for the acoustic pressure field using this equation requires a rapid means of evaluating the eigenvalues, k_n , and the eigenvectors, $Z_n(z)$, of the equation

$$d^2Z/dz^2 + [\gamma^2(z) - k^2] = 0$$

For the remainder of this section, $P(z) = Z(z)$. Since

$\gamma(z) = \omega/\alpha(z)$, where $\alpha(z)$ is the vertical sound speed profile, the equation to be solved can be written

$$d^2P/dz^2 + (\omega^2/\alpha^2 - k^2)\cdot P = 0 \qquad \text{T.8}$$

The computational means chosen to solve this equation is the propagator-matrix method first developed by Thomson [*1950*] and Haskell [*1953*]. Following their treatment, the vertically heterogeneous ocean is replaced by a stack of homogeneous layers overlying a homogeneous half-space.

Rewriting equation T.8 as a pair of coupled first-order ordinary differential equations gives:

$$dP/dz = X$$
$$dX/dz = \omega^2 P\cdot(k^2/\omega^2 - 1/\alpha^2)$$

Defining $b_1 = X$ and $b_2 = \omega P$ and the vector $\mathbf{b} = (b_1 , b_2)$, then

$$\mathbf{db}/dz = \omega\mathbf{Ab}$$

with $$\mathbf{A} = \begin{bmatrix} 0 & (1/c^2 - 1/\alpha^2) \\ 1 & 0 \end{bmatrix}$$

where c, the horizontal phase velocity, equals ω/k and is the eigenvalue, or the desired root, of the equation for **b**.

The ocean is modeled as a stack of homogenous layers with $h(\alpha) = 1/c^2 - 1/\alpha^2$ constant in each layer. In this model, the vector **b** satisfies

$$\mathbf{b}(z) = \exp[\omega \mathbf{A} d]\cdot\mathbf{b}(z_0) = \mathbf{P}(z,z_0)\mathbf{b}(z_0)$$

where d is the thickness of the layer, $d = z - z_0$

$\mathbf{P}(z,z_0)$ is the matrix "propagator"

The matrix coefficients of the propagator can be evaluated by Sylvester's theorem to give

$$\mathbf{P}(z,z_0) \equiv \exp[\omega \mathbf{A} d] = \begin{bmatrix} c(\alpha) & h(\alpha)s(\alpha) \\ s(\alpha) & c(\alpha) \end{bmatrix}$$

where the coefficients of the propagator are

$c(\alpha) = \cos[\omega d\sqrt{-h(\alpha)}\,]$ & $s(\alpha) = -\sin[\omega d\sqrt{-h(\alpha)}\,]/[\sqrt{-h(\alpha)}\,]$

if $h(\alpha)<0$ (that is, if P(z) is oscillatory in the layer) and

$c(\alpha) = \cosh[\omega d\sqrt{h(\alpha)}\,]$ & $s(\alpha) = -\sinh[\omega d\sqrt{h(\alpha)}\,]/[\sqrt{h(\alpha)}\,]$

if $h(\alpha)>0$ (that is, if P(z) is exponential in the layer).

Given a starting solution at some depth, we can propagate the

solution to the surface using this formula.

The primary approximation made in this realization of the propagator-matrix method is that the vertical sound speed profile, $\alpha(z)$, can be adequately modeled as a stack of homogeneous layers. This is an approximation that is made for many numerical solutions to the problem of sound propagation through a waveguide. To insure that discretizing the ocean is valid here, we choose a layer thickness that is a fraction (typically 1/2) of the smallest vertical wavelength in the oscillatory region. For the frequencies and profiles used here, this layer spacing is typically about 10 meters. (Choosing spacing finer than this has no significant effect on the result.) Although the ocean is approximated as a stack of homogeneous layers for purely computational reasons, it is worth noting that this approximation is not necessarily unrealistic. There is evidence that in many regions of the ocean, such as the Arctic, the density profile can exhibit regular step-like characteristics [*Brekhovskikh and Lysanov, 1982*].

The basic algorithm for finding the eigenvalues at a given frequency, ω, is to choose a value of c_0, compute a starting solution and propagate to the surface. Along the way, the number of zero-crossings in pressure (in b_2, that is) is kept track of. If the value of b_2 at the surface is 0, then a root, with the number of zero-crossings determining the mode number. If b_2 is not 0, a new value for the phase velocity, say c_1, is chosen and the process is repeated, with $\mathbf{b}$ again propagated to the surface. If the value of

b_2 has changed sign, the root lies in between c_0 and c_1 and can readily be determined using an interpolation/bisection scheme for choosing new starting values for c.

Using this method, all of the roots at this frequency can be isolated quickly. If the layer spacing is less than or equal to half a vertical wavelength, then there can be at most one zero-crossing in a layer. In that case, the total number of zero-crossings (the mode number) can be rapidly calculated by checking the value of b_2 at the interface of each layer for a change in sign.

Since the vertical eigenfuctions are computed during the course of these calculations, it is easy to find the modal amplitude factor, which is proportional to $Z_n(z_s) \cdot Z_n(z)$ -- the product of the eigenfunction evaluated at the source, z_s, and at the receiver, z. In this thesis, this amplitude factor will be called the "excitation" of the mode, for it determines the degree to which one mode is excited relative to another for a given source-receiver configuration. Vertical wavefunctions, P(z), for a near-linearly increasing sound-speed profile (Figure 4.2) are exhibited in Figure 2.2. As can be seen, higher modes sample deeper in the ocean.

As described in Appendix One, the computed vertical eigenfunctions can be used in a variational principle calculation to yield an exact value of the group velocity, without resorting to numerically differentiating phase velocities. This method also yields the derivatives of phase and group velocity with respect to sound speed in each layer, which can be used in the tomographic

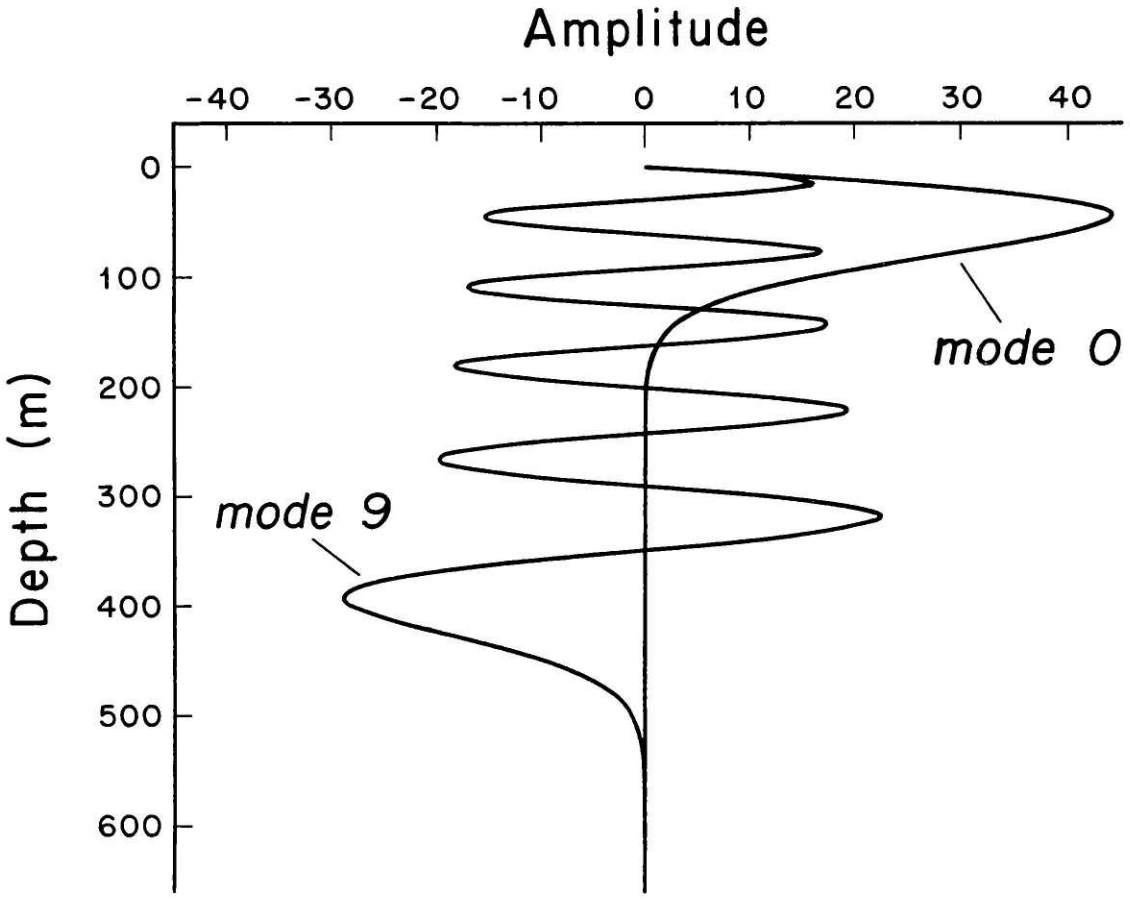

Figure 2.2. Vertical displacement fields of Mode 0 and Mode 9 for a nearly linearly increasing sound speed profile. The absolute amplitude (horizontal axis) is arbitrary.

inverse procedure of determining sound speed from arrival times.

For broadband sources, the eigenvalues will have to be determined at a number of frequencies. A root, c, at one frequency, ω, can be used to predict a new root, $c+\delta c$, at a nearby frequency, $\omega+\delta\omega$, using the relationship

$$\delta c/\delta\omega = (c/\omega)(1 - c/u)$$

This linear extrapolation makes use of the group velocity, u, calculated at ω. If the roots and group velocities at two previous frequencies have been computed, then cubic extrapolation usually gives the roots at the new frequency very accurately before the root-isolation algorithm has even been used. With the modal phase velocities, group velocities, and excitations calculated for a variety of frequencies across the bandwidth, the synthetic acoustic arrival pattern can now be constructed.

The phase and group velocities are used to calculate the phase velocities at the Fast Fourier Transform (FFT) points using cubic spline interpolation. The modal excitations are also interpolated at the FFT points. The pressure field, p(r,z), at the FFT frequencies is then calculated as a sum over modes using formula T.7. A Fourier transform to the time domain yields the acoustic impulse response time series. This is then convolved with the source function and low-pass filtered. Finally, the carrier frequency is removed by complex demodulation to produce the

envelope function of the final synthetic arrival pattern [*Brown, 1981*]. Figure 3.4 shows the envelope of a synthetic normal mode arrival pattern or sonogram calculated for a typical mid-latitude profile.

The attenuation of sound intensity in water at the frequencies of interest is approximately given by [*Brekhovskikh and Lysanov, 1982*] $0.1f^2$ [dB/km], where f is the sound frequency in kHz. At the ranges considered here, the attenuation is only a few dBs and will be neglected throughout this thesis.

2.3 The Adiabatic Approximation

So far only vertically stratified range-independent sound-speed fields -- in which sound speed varies with depth alone -- have been considered. In the ocean, however, sound speed also varies laterally. This range dependence can significantly affect the acoustic arrival pattern.

The adiabatic approximation is used here as a first attempt at estimating the effects of range dependence. This appears to be adequate to account for the range-dependence in the RTE83 experiment. This approximation involves treating the ocean as having a nearly-stratified sound-speed field -- one whose vertical waveguide is slowly varying in the horizontal direction. A precise quantitative description of the region of validity of the adiabatic approximation is difficult to determine [*Desaubies, 1984*]. Qualitatively, however, the main idea is that for a given ray, or for a mode that comprises that ray, the cycle range of the ray (typically 30 to 50 kilometers) must be small compared with the scale of the horizontal variation of the sound-speed field [*Brekhovskikh and Lysanov, 1982*].

If the horizontal changes in the vertical waveguide are gradual enough, coupling between the normal modes may continue to be neglected, but in the adiabatic approximation, the local acoustic wavefunctions are retained. For this reason, this approximation is sometimes called the "local mode" approximation.

Recalling equation T.7, in the calculation of the arrival pattern in the range-independent case, the pressure, P, at range, r, source depth, z_s, and receiver depth, z, can be written as a sum over normal modes:

$$P(r,z) = (i/4)\cdot\sum_{n} H_0^{(1)}(k_n r)\cdot Z_n(z_s)\cdot Z_n(z)$$

In the range-independent case, the range-averaged sound speed field is used to calculate the elements of the right-hand side of this equation. The adiabatic approximation does not involve adding new terms to the right hand side of the equation, but instead it involves an improvement in the calculation of both the excitations and the horizontal wave number. In this approximation, the vertical wavefunctions are calculated and evaluated locally. That is, $Z_n(z_s)$ is calculated for the sound speed profile of the source (if it is known), rather than for the range-averaged profile. Similarly, $Z_n(z)$ is calculated for the sound speed profile of the receiver (if it is known).

If vertical sound speed profiles are available for the entirety of the range of the experiment, then the adiabatic horizontal wave number is calculated by taking a weighted average of the horizontal wave numbers calculated for each of the profiles. The weights depend on the fraction of the range covered by the particular local profile. The horizontal wave number is

determined from the local phase velocities through the relationship $k_n=\omega/c_n$.

The computer-time-consuming effort of calculating the eigenvalues for several profiles can be avoided in the case when the perturbations in phase velocity are sufficiently small to allow the use of linear perturbation theory. In that case, as will be shown, the adiabatic horizontal phase velocity is the same as that calculated in the range-averaged case.

In the linear regime, the perturbations δc in modal phase velocity can be calculated from perturbations $\delta\alpha_i$ in sound speed in layer i as follows:

$$\delta c = \sum_i (\delta c/\delta\alpha_i)\cdot\delta\alpha_i$$

Now, consider two sound speed profiles, α_1 and α_2, that differ in only a single layer, i=n, having values in that layer of α_{1n} and α_{2n}, respectively. Imagine that the two profiles extend over arbitrary fractions of the total range, A and B, such that the range-averaged sound speed in that layer is $\alpha_n = A\alpha_{1n} + B\alpha_{2n}$ where $A+B=1$.

Then, in the linear adiabatic approximation:

$$\Delta c_1 = (\partial c/\partial\alpha_n)(\alpha_{1n} - \alpha_n)\ , \qquad \Delta c_2 = (\partial c/\partial\alpha_n)(\alpha_{2n} - \alpha_n)$$

Therefore, in this approximation, the total weighted perturbation, Δc, is

$$\begin{aligned}\Delta c &= A\Delta c_1 + B\Delta c_2 \\ &= (\partial c/\partial \alpha_n)[A(\alpha_{1n} - \alpha_n) + B(\alpha_{2n} - \alpha_n)] \\ &= (\partial c/\partial \alpha_n)[A\alpha_{1n} + B\alpha_{2n} - \alpha_n(A+B)] \\ &= (\partial c/\partial \alpha_n)[\alpha_n - \alpha_n] \\ &= 0\end{aligned}$$

That is, for the case of two profiles that vary in a single layer, the phase velocity calculated in the linear adiabatic approximation is the same as the phase velocity calculated in the range-averaged case. This result generalizes easily to multiple profiles (since multiple profiles can be considered as two-profile groupings) and to perturbations in multiple layers (since the sum over layers separates).

2.4 Ice Layer

During the winter, much of the Greenland Sea can be covered with 10 centimeters of ice or more. Modeling the propagation of sound through ice requires accounting for compressional waves and shear waves. Figure 2.3 shows the coordinate system that will be used in this section. This is the air-water coordinate system shown in Figure 2.1 with an ice layer of constant thickness d placed on top.

The density of ice is ρ_1, and of water, ρ_0. The ice has a compressional wave speed, α. Water supports only compressional waves; it cannot support a shear stress. Yet perfectly elastic, isotropic sound waves in a solid require another variable, the rigidity μ, to be adequately described. The rigidity is defined as $\mu=\rho_1\beta^2$ where β is the bulk shear wave speed. All the quantities describing the ice will be taken to be constants.

Sound originates in water at depth, z_s, and, as before, only sound propagating through water (and ice) along the r-z plane will be considered. Sound traveling in the r-z plane in the water will not excite horizontally-polarized Love waves in a homogeneous ice layer of constant thickness. Moreover, Love waves excited in the ice would not couple into the water because water does not support a shear stress. So Love waves will be neglected here.

The remaining problem is to solve for the propagation of Rayleigh waves, which are composed of compressional waves and vertically-polarized waves whose independent motion are not

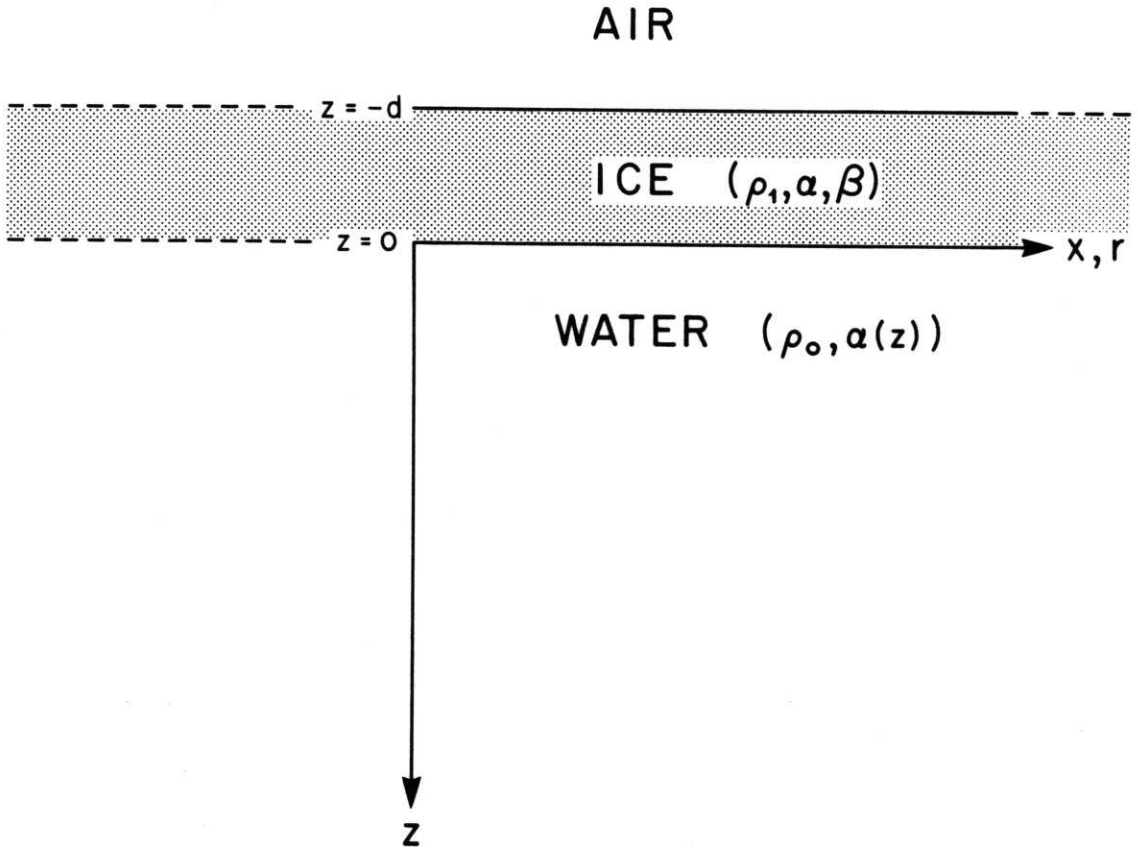

Figure 2.3. The air-ice-water coordinate system. The density of ice is ρ_1, and α and β are the compressional and shear wave velocities of sound in ice. The density of water is ρ_0 and the vertical sound speed profile in water is $\alpha(z)$.

separable for horizontal propagation in a layered medium.

To treat the propagation of Rayleigh waves in ice, four variables are needed, rather than the two used in water. The discussion in this section follows Takeuchi and Saito [*1972*] and Woodhouse [*1980*], although the variables of the latter are used here. They are

Y_1 -- the vertical displacement, u(z)

Y_2 -- the tangential displacement, u(r)

Y_3 -- the vertical stress, τ_{zz} (here, τ_{zz}/ω is actually used)

Y_4 -- the tangential stress, τ_{zr} (here, τ_{zr}/ω)

where τ_{zz} and τ_{zr} are components of the stress tensor, $\boldsymbol{\tau}$.

When the vertical eigenfuction is propagated from the bottom of the ocean through the water, the ice-water boundary conditions are required to continue the solution into the ice. The interface conditions are:

1) Continuity of verticle particle displacement

$$u(z=0+) = u(z=0-) = u_0$$

2) Continuity of vertical stress

$$\tau_{zz}(z=0+) = \tau_{zz}(z=0-) = \tau_{zz0}$$

3) Vanishing of horizontal stress

$$\tau_{zr}(z=0) = 0$$

Appendix Two will go into some of the computational details of propagation in the ice, including an elaboration of how the variables transform from the water vector **b** to the ice vector **Y**. The above interface conditions give a starting solution for the Rayleigh vector at the bottom of the ice of $(u_0\ ,\ 0,\ \tau_{zz0}\ ,\ 0)$.

A second, independent, starting solution for Rayleigh waves exists. There can be a discontinuity in the horizontal, or tangential, displacement, u(r,z=0). This "free slip" condition gives a starting vector of (0, Q, 0, 0) where Q is the arbitrary slip.

These two solutions are propagated to the surface of the ice using the equations of motion. The two surface solutions are then summed, to give the total solution, and the value of Q is determined by the condition at the ice-air interface that the horizontal and vertical stresses vanish.

As in the water, the equations of motion to be solved can be written in the form

$$\partial \mathbf{Y}/\partial z = \omega \mathbf{A} \mathbf{Y}$$

Matrix **A** is of the form:

$$\mathbf{A} = \begin{bmatrix} 0 & p(1-2\mu/\sigma) & 1/\sigma & 0 \\ -1/c & 0 & 0 & 1/\mu \\ -\rho_1 & 0 & 0 & 1/c \\ 0 & -\rho_1+4\mu p^2(1-\mu/\sigma) & -p(1-2\mu/\sigma) & 0 \end{bmatrix}$$

ρ_1 is the density

$\sigma=\lambda+2\mu$, where λ and μ are Lamé parameters (μ is the rigidity)

p is the inverse phase velocity, $p=1/c=k/\omega$

This form of the equations reduces to the fluid equations if $Y_1=b_1$ and $Y_3=-\rho_0 b_2$ (see Appendix Two).

The ice layer has a propagator-matrix derived from the matricized equation of motion, just as the water does, although it is numerically more complicated. If the two independent solutions at the top of the ice are called $(Y_{11}, Y_{12}, Y_{13}, Y_{14})$ and $(Y_{21}, Y_{22}, Y_{23}, Y_{24})$ then a mode is found whenever the determinant $Y_{13}Y_{24} - Y_{23}Y_{14}$ is zero. Since the compressional and shear velocities in the ice are much greater than the speed of sound in water, the wavefunctions are purely exponential in the ice. This means that there cannot be more than one zero-crossing of the determinant in the ice. (Numerical instability in this method requires a slightly more complicated approach discussed in

Appendix Two.)

Without the ice layer, the roots were isolated by propagating the vector **b** to the surface at two different phase velocities, c_1 and c_2 , and seeing if the value of the pressure, b_2 , has changed sign. The procedure with the ice layer is the same, but now the determinant given above is examined for a sign change. Once the modal roots, group velocities, and excitations are calculated for a variety of frequencies over the bandwidth of interest, the calculation of the acoustic arrival pattern is carried out as before. The effect on the acoustic arrival pattern of the modes locked into the ice will be considered in Chapter Four.

2.5 Group-velocity Inversions

So far, only the acoustic forward problem has been examined -- the determination of modal group velocities and of the entire acoustic arrival pattern from a knowledge of vertical (and perhaps horizontal) sound speed information. This is useful for experiments in which the local ocean conditions have been studied, perhaps to help track objects in the ocean from the sounds they emit. In situ measurements of temperature and salinity can be used to calculate such sound speed data.

In tomographic experiments, instruments are placed at the edge of water masses, and sound is sent through in an effort to gain information about the ocean conditions. In these cases, the group velocities (arrival times) and the acoustic arrival pattern are what is measured, and the sound speed profile -- and hence density, temperature, and salinity information -- is what is desired. For this, linear inverse theory is used.

The first inverse problem to be examined is the determination of sound speed from modal group velocity data. Suppose the arrival time, t_i, of mode i can be determined at a given frequency. If the range, r, is known, the group velocity, u_i is simply r/t_i. To use this data to solve for the sound speed in a layer l of the ocean requires knowledge of the derivatives of group velocity with respect to sound speed in that layer -- $\partial u_i/\partial \alpha_l$. These so-called group velocity kernels, G_{il}, are not difficult to calculate, as is

discussed in Appendix One.

If a one-layer ocean of sound speed α has modal group velocity u_i, and a slightly different ocean has sound speed $\alpha_0 = \alpha - \delta\alpha$ and modal group velocity $u_{0i} = u_i - \delta u_i$, the Taylor series expansion of the group velocity u_i can be written as:

$$u_i = u_{0i} + (\partial u_{0i}/\partial\alpha)\cdot\delta\alpha + \ldots$$

The solution of the linear forward problem (δu_i unknown) would be

$$\delta u_i = (\partial u_{0i}/\partial\alpha)\cdot\delta\alpha$$

and the solution of the linear inverse problem ($\delta\alpha$ unknown) would be

$$\delta\alpha = \delta u_i\cdot(\partial u_{0i}/\partial\alpha)^{-1}$$

The inverse problem, even in the single layer case, requires a starting sound speed model to calculate the kernels. Moreover, for the first derivatives to be useful, the starting solution, α_0, must be close to the actual ocean, α, so that their difference, $\delta\alpha$, is sufficiently small. This is the so-called linear regime.

A starting model can be determined using in situ velocity data taken at the beginning of an experiment or historical data or both.

In any case, assume for now that there is a reasonable starting model. Ultimately, the inverse procedure will be able to provide some means of evaluating the starting model. For instance, if the inverse fails to provide a realistic solution, it may be because the starting model was poor.

Given a starting sound speed model, $\alpha_0(z)$, divided into layers α_{0l}, both the expected normal mode group velocities, u_{0i}, and the group velocity kernels, $G_{il}=\partial u_{0i}/\partial\alpha_{0l}$ can be calculated. With observed or measured group velocities, u_i, the data takes the form:

$$\delta u_i = u_i - u_{0i}$$

and the problem takes the form of a sum over all the layers, l, of the ocean

$$\delta u_i = \sum_l G_{il}\cdot\delta\alpha_l \qquad \text{T.9}$$

where the unknowns to be solved for, $\delta\alpha_l$, are the difference between the actual ocean, α_l, and the starting or model ocean, α_{0l}. So $\alpha_l=\alpha_{0l}+\delta\alpha_l$. In the case of the group velocity inversions, there are usually fewer data than unknowns ($i<l$) so the problem is underdetermined.

Of course, in any real world problem, there will be errors associated with the modal group velocity measurements. Because

the actual statistical variation of the measurements is not generally well known, the data are assumed to be statistically independent with associated individual errors that have a Gaussian distribution of zero mean and standard error, σ_i. This assumption allows the analysis of the linear inverse problem to be carried out exactly, following Parker [*1977*]. The numerical solution Parker describes, a so-called spectral expansion, follows Gilbert [*1971*].

There is another potential source of error in the data. In the model ocean, the group velocity of each mode is determined explicity with great accuracy. So it is usually not difficult to identify peaks in the synthetic arrival pattern with modes in the starting ocean. The key to the group-velocity inversion procedure, however, is to relate peaks in the observed acoustic arrival pattern with modes in the actual ocean. If these modes are misidentified, their arrival times will be miscalculated and the left hand side of T.9 will be in error. The difficulty of identifying distinct modes in the observed arrival pattern will be discussed in Chapter Five. For now, errors associated with the misidentification of modes will be lumped in with the zero-mean Gaussian measurement errors.

If the data are reasonably accurate, at least one solution -- the actual ocean -- exists. The finiteness of the data and the presence of error in the data implies that there will probably be many solutions. One of the key tasks in "model construction" is

determining criteria for choosing one solution from among all the possibilities.

To solve T.9, divide both sides of the equation by the associated errors -- weighting both the data and the group velocity kernels:

$$\delta\tilde{u}_i = \delta u_i/\sigma_i$$
$$\delta\tilde{G}_{il} = G_{il}/\sigma_i$$

This weighting creates dimensionless data with unit variance and allows the more accurate data to count more than the inaccurate data.

Rewriting Equation T.9 with the new variables yields:

$$\delta\tilde{u}_i = \sum_l \tilde{G}_{il}\cdot\delta\alpha_l \qquad \text{T.10}$$

The model construction problem is to solve for $\delta\alpha_l$ given group velocity data, kernels, and errors.

In Parker [*1977*], the sum over l here and in the equations that follow are written as integrals over z. The computational approach used in this thesis divides the ocean into homogeneous layers, and the integrals can be rewritten as sums that extend over the same depths. This allows the integrals to be approximated numerically. The matrix, **G**, for instance, consists

of rows that correspond to group velocity kernels in different layers for a particular mode.

The means of solving T.10 used here essentially involves forming $\mathbf{G}^T\mathbf{G}$, a square version of the $\tilde{\mathbf{G}}$ matrix, and then finding its inverse so that the $\delta\alpha_l$ can be isolated. The matrix inversion is accomplished by a standard eigenvector-eigenvalue decomposition technique. The square matrix Γ is called the Gram matrix, and its elements are

$$\Gamma_{ij} = \sum_l \tilde{G}_{il} \cdot \tilde{G}_{jl}$$

Since Γ is positive definite and symmetric, it has no negative eigenvalues. It can be diagonalized with orthogonal matrix $\mathbf{O}$:

$$\mathbf{O}^T\Gamma\mathbf{O} = \Lambda$$

where Λ is a diagonal matrix of the eigenvalues of Γ in descending order starting with the largest eignvalue, λ_1, in the Λ_{11} position and ending with the smallest, λ_n, in the Λ_{nn} position. Assuming that the rows of $\tilde{\mathbf{G}}$ are not linearly dependent, none of the eigenvalues are zero. The eigenvalues λ_1 to λ_n are referred to as the spectrum of the problem.

To solve T.10, define functions Ψ with elements

$$\Psi_{il} = \lambda^{-1/2} \sum_j O_{ji} \cdot \tilde{G}_{jl}$$

The rows of Ψ are an orthonormal set:

$$\sum_l \Psi_{il} \Psi_{jl} = \delta_{ij}$$

Expanding $\delta\alpha_l$ in terms of these orthogonal functions yields

$$\delta\alpha_l = \sum_i a_i \cdot \Psi_{il} \qquad \text{T.11}$$

where

$$a_i = \sum_l \Psi_{il} \cdot \delta\alpha_l$$

$$= \lambda_i^{-1/2} \sum_j O_{ji} \cdot \tilde{u}_j \qquad \text{T.12}$$

These coefficients, a_i, are statistically independent with standard error $\lambda_i^{-1/2}$. Since the eigenvalues decrease with increasing i, the expansion T.11 is in functions whose coefficients increase in uncertainty and magnitude. Trying to fit the original data more precisely by adding in more eigenvalues in T.11 usually makes the solution more oscillatory, and therefore, to some extent, more unrealistic, at least in the case of relatively smooth sound-speed profiles.

In general, some criterion must be established for either truncating the series in T.11, or giving diminished weight to the higher terms (smaller eigenvalues). Either of these methods means that the solution will not exactly fit the original data, but this is reasonable, given the random errors associated with the data. Truncation is used here, and one simple way of disregarding the undesirable, oscillatory eigenvectors is to use the squared two-norm misfit to the data, χ^2, defined as

$$\chi^2 = \sum_i (\delta\overline{u_i} - \delta\tilde{u}_i)^2$$

where $\delta\overline{u_i}$ is obtained by substituting the truncated series into the right hand side of T.10.

Rewriting in terms of the eigenvalues and coefficients yields

$$\chi^2 = \sum_j \lambda_j \cdot (a_j)^2 \qquad \text{T.13}$$

where the sum is over the truncated terms -- those not added into T.11.

As more and more terms are added into T.11, χ^2 gets smaller and smaller, although at a diminishing rate. Since the weighted data, $\delta\tilde{u}_i$, has unit variance, χ^2 is reduced to its expected value -- the number of degrees of freedom in the truncated model, which can be regarded as the number of independent data.

The exact truncation scheme used is not crucial to this solution, as long as the inversion yields a model that is closer to the actual ocean than the starting model. If that is the case, new group velocities can be computed in the new model, and a new inversion done. This process may be iterated until the group velocities are all within the error bars of the observed data. If the starting model is based on temperature and salinity data taken at the beginning of a tomography experiment, the difference between the actual ocean and the starting model should never be more than about 0.5 meter per second in any layer, which is close to the linear regime.

In the linear regime, the χ^2 truncation scheme should yield an acceptable solution after a single inversion. Close to the linear regime, it may be best to truncate the model even sooner, while the eigenvalues are large and coefficients, a_i, are small, so that short, incremental steps are taken toward the solution. This scheme may require two or three iterations to achieve an acceptable solution.

Achieving an acceptable solution is a necessary but not sufficient condition to achieving the correct solution. There is no way of being sure the answer obtained from the inversion is correct. Nevertheless, experience with inversions and with historical sound speed data can increase confidence in the solution. Sometimes there is enough historical data to indicate that the sound speed profiles in a localized region, like the

Greenland Sea, exhibit consistent patterns during certain times of the year. For instance, during the spring, the water temperature in the Greenland Sea tends to be very uniform. This near-adiabatic condition results in a sound speed profile that increases nearly linearly with depth. Throughout the summer, the surface is warmed slightly, creating a sound speed minimum at about 100 meters. Tomographic inversions that do not agree with these historical trends would be very suspect. If enough historical data exists, it is possible to statistically quantify the likely variations in sound speed. This information can be used in the inversions to directly limit the solutions.

Suppose there are many historical profiles, $\alpha_i(z)$, i = 1 to n. If the average of the n profiles is computed, then each profile can be described as a perturbation $\delta\alpha_i(z)$ to that average. It may very well be the case that most of the variation of these n perturbations can be described by a very few orthogonal functions, called empirical orthogonal functions (EOFs).

To find out if the historical sound speed data in a region can be well described by a few EOFs involves decomposing the data into eigenvectors using a method very similar to the inversion technique described above. In this case, the derived orthonormal functions are the EOFs. The EOF analysis is, in this sense, a form of data compression. This analysis was carried out for historical spring Greenland Sea Profiles, and the results are described in Chapter 5.

The EOF analysis can do more than just quantify the historical variation of the ocean in a region. The EOFs themselves can be used in the inversion procedure. The group-velocity kernel in a layer can be multiplied by the value of the EOF in the layer and this product can be summed over all the layers. Now, using essentially the same inversion technique described above, the quantity being solved for are the amplitudes of a few EOFs -- rather than the sound-speed perturbation in many layers. The new model is then the starting model (the average profile) plus the EOFs weighted by their amplitudes. In general there will be fewer EOFs than layers needed to describe a given sound speed profile adequately. So, usually much fewer data are required in the "EOF" inversion than in the "layer" inversion.

2.6 Multiple Receivers and Mode Filtering

Besides using EOFs, another way to aid the job of constructing a model of the ocean is to use multiple acoustic receivers. An actual experiment could make use of 6 or more receivers spaced tens of meters apart along a mooring. Although the phase and group velocity of a mode are not a function of depth for a given range-independent sound speed field, the excitation of that mode is depth dependent. Judicious placement of the receivers will yield arrival patterns that emphasize different vertical modes. In the case of the near-linearly increasing sound speed profile of Figure 4.2, shallow receivers emphasize the lower

order modes. Multiple receivers can therefore be used to aid the process of identifying different modes and determining when they arrive. This process, which is crucial to determining the data for the inversion procedure, can be made particularly simple if the starting model is very close to the actual ocean. The idea then is to use the string of receivers at different depths as a vertical array and isolate individual modes.

Consider the observed undemodulated acoustic arrival patterns of a two receiver array. Let those arrival patterns be deconvolved with the source function and written as $\tilde{P}_1(t)$ and $\tilde{P}_2(t)$. Suppose it is known that a certain portion of those arrival patterns, $P_1(t)$ and $P_2(t)$, consists solely of the contribution from normal modes zero and one. Then, if these two functions of time are Fourier-transformed into complex functions of frequency, $P_1(\omega)$ and $P_2(\omega)$, they can be written as a sum of these two normal modes as follows:

$$P_1(\omega) = A_{11}(\omega)\exp\{i\cdot[k_1(\omega)r-\Phi]\} + A_{12}(\omega)\exp\{i\cdot[k_2(\omega)r-\Phi]\}$$
$$P_2(\omega) = A_{21}(\omega)\exp\{i\cdot[k_1(\omega)r-\Phi]\} + A_{22}(\omega)\exp\{i\cdot[k_2(\omega)r-\Phi]\}$$

where k_n is the horizontal phase velocity of mode n

r is the range

$\Phi = \omega t_0 + \pi/4$

t_0 is the starting time for the arrival pattern

A_{mn} is the excitation of mode n at receiver m.

These equations may be rewritten in matrix format as

$$\mathbf{P}(\omega) = \mathbf{A}(\omega)\mathbf{c}(\omega)$$

where $c_n(\omega) = \exp\{i\cdot[k_n(\omega)r-\Phi]\}$

This makes use of the asymptotic form of the Hankel function. Recalling the discussion from Section 2.2, the excitation factor is proportional to the vertical wavefunction evaluated at the receiver. If the excitation factors of each mode at the two receivers were known as a function of frequency, then all of the elements A_{mn} of the excitation matrix, **A**, would be known. In that case, $\mathbf{A}(\omega)$ would be inverted and the value of the mode at those frequencies -- the complex exponential $c_n(\omega)$ -- could be isolated. Once the value of the complex exponentials for a given mode are known at a variety of frequencies across the bandwidth, they may be Fourier transformed back into the time domain. The resulting time series is the arrival pattern of an individual mode.

Of course, the true excitations of modes zero and one in the ocean cannot be known unless the actual vertical sound speed profile is known. Yet, if the starting model is similar to the true ocean, then the excitations of the mode in the starting model may be sufficiently close to the true excitations to be used to make up the **A** matrix. In that case, using the observed arrival patterns

and the calculated excitations, individual modes in the actual ocean can still be isolated.

This procedure may be generalized to an arbitrary number of modes, n, as long as there are at least as many modes as receivers, and as long as there is a limited interval of the received arrival patterns that is made up exclusively by those n modes and no more. If there are too few receivers, or if there is energy in the interval from other modes, then the n modes cannot be isolated unambiguosly using this procedure. Six receivers are used in the synthetic experiment of Chapter Five to isolate modes 0 to 4 from the observed data. Figure 5.6 shows that this technique can allow the unambiguous identification of the arrival time of individual modes, in this case mode 4.

This technique will work whenever the shape of the vertical sound speed profiles for the true ocean and the starting model are very similar, since in that case the modal excitations will be nearly the same for the two profiles (except for a constant amplitude and phase factor that does not affect the result of the matrix inversion). In general, however, the starting model will not have the same shape as the true ocean. It is more likely that one or more group velocity inversions of the kind described in the previous section would first be required to get close enough to use this mode isolation or mode filtering procedure. This is the case for the synthetic experiment of Chapter Five.

2.7 Signal Transmission and Processing

Crucial to the tomography experiments described in this thesis are the characteristics of the source signal and the signal processing at the receiver. The treatment of the acoustic signal in this section will follow Howe [*1986*] closely. The RTE83 400-Hz experiment described in Chapter 3 will be used as an example, although the discussion generalizes easily to the 250-Hz experiment planned for the Greenland Sea.

The source level was 174 dB re 1 µPA at 1 m. As is typical of acoustic sources, the amount of peak power that can be put in the water is mechanically and electrically limited. Therefore, the energy a single pulse of a given length can contain is also limited. To overcome spreading and absorption loss, and achieve both an adequate signal-to-noise ratio and high travel-time resolution, pulse-compression techniques were used (in conjunction with the use of a broad-band and relatively low frequency signal).

It is possible to achieve the same effect of sending a single strong pulse by using a periodic pulse compression waveform. Each period of that waveform consists of a set of L individual phase-modulated pulses. The right modulation will allow the energy contained in the L pulses to be collapsed into a much more energetic equivalent single pulse [*Metzger, 1983*]. Here, the transmitted signal is made up of periodic repititions of a linear-maximal, pseudo-random sequence with the following characteristics:

carrier frequency f_0 = 400 Hz (exactly)

digit length = 4 cycles of 400 Hz = 0.01 s

sequence length = L = 511 digits = 5.11 s

transmission length = 24 sequence periods = 122.64 s

modulation phase angle $\theta_0 = 87.408^0$.

The transmitted signal may be considered to be composed of single digits in the linear maximal sequence. Each digit is defined as $\sin(2\pi \cdot f_0 \cdot t \pm \theta_0)$, where t=0 is the beginning of a digit and a positive (negative) phase shift corresponds to a logical '1' ('0') in the linear maximal sequence. The particular phase angle given above optimizes the signal-to-noise (SNR) ratio, and this code can be processed to yield an output waveform without sidelobes.

The received signal is complex demodulated and sampled at 200 Hz or two samples per digit. A coherent average is formed of the middle 22 sequence periods (to avoid end effects, the first and last periods are not included in this average). The received SNR increases directly with the number of sequence periods taken in the coherent average [*Metzger, 1983*]. Two interleaving sequences are constructed, each consisting of one sample per digit. These two sequences are then individually correlated with a replica of the transmitted sequence. Last, they are recombined to give the processed arrival pattern.

The *rms* travel time precision σ_0 associated with the correlation peak is greater than or equal to $\sigma_{peak}(SNR)^{-1/2}$ where σ_{peak} is the *rms* width of the peak. Typical values of

σ_{peak} and SNR in the RTE83 experiment were 5 ms and 20 dB, respectively, which gives a lower bound of 0.5 ms for σ_0.

What can be measured physically from a pulse with a travel time of about 200 seconds (300 km range) whose arrival time can be measured with a precision of perhaps 1 millisecond? If the travel time can be measured to better than one part in 10^5, then the speed of sound can be measured to better than one part in 10^5 -- or about 0.01 m/s. As discussed earlier, this in turn suggests that range-averaged temperature changes of the order of a few thousandths of a degree Celsius can be observed, in theory. In fact, typical temperature disturbances -- so-called mesoscale ocean features -- tend to be localized in range and depth. Therefore, they only interact with part of the acoustic signal -- perhaps one ray out of an entire arrival sequence -- and then only over a portion of the trajectory of that ray -- perhaps only near the surface. In that case, it is more likely that temperature changes of the order of a tenth of a degree would be measured. Chapter Five will focus on what level of sensitivity and resolution of temperature might be achievable using modal tomography in the Greenland Sea.

The key point is that the signal-processing scheme described in this section allows the acoustic signal emitted from the source to be treated as a single energetic pulse. Therefore, this scheme allows the recovery of the entire spread-out signal at the receiver as depicted in Figure 3.3. For this reason, the group velocity of individual acoustic wave packets -- rays -- (and, in some case,

individual modes) can be monitored separately. These wave packets sample different portions of the ocean between the source and receiver. As their individual arrival patterns are monitored over time, the range- and depth-dependent variation of sound speed and therefore temperature can be deduced. This is what makes tomography possible.

3. THE RTE83 EXPERIMENT

The first application of normal modes will be a comparison of normal mode theory with WKBJ and ray theory and with measured pulse arrival patterns at 300 kilometer range in the Atlantic. This will serve simultaneously as a check on the accuracy of the normal mode program and as a test of the usefulness of normal modes in the mid-latitudes.

The 1983 Reciprocal Acoustic Transmission Experiment [*Worcester, et al, 1985*] was carried out at 32^0 N, 70^0 W, near Bermuda. The position of the two moorings is shown in Figure 3.1. The moorings were placed near the depth of the sound channel, 1300 m, and at a separation of 300 km. The reference sound speed profile over this region is shown in Figure 3.2. This reference profile was derived from expendable bathythermograph (XBT) casts taken at the time of the experiment combined with historical data on deep-ocean salinity and temperature. All 13 resolved rays are also shown in Figure 3.2, which has an exaggerated vertical scale to allow the rays to be distinguishable.

The transmitted pulse was centered at 400 Hz and had approximately 10-millisecond resolution. Figure 3.3 displays the

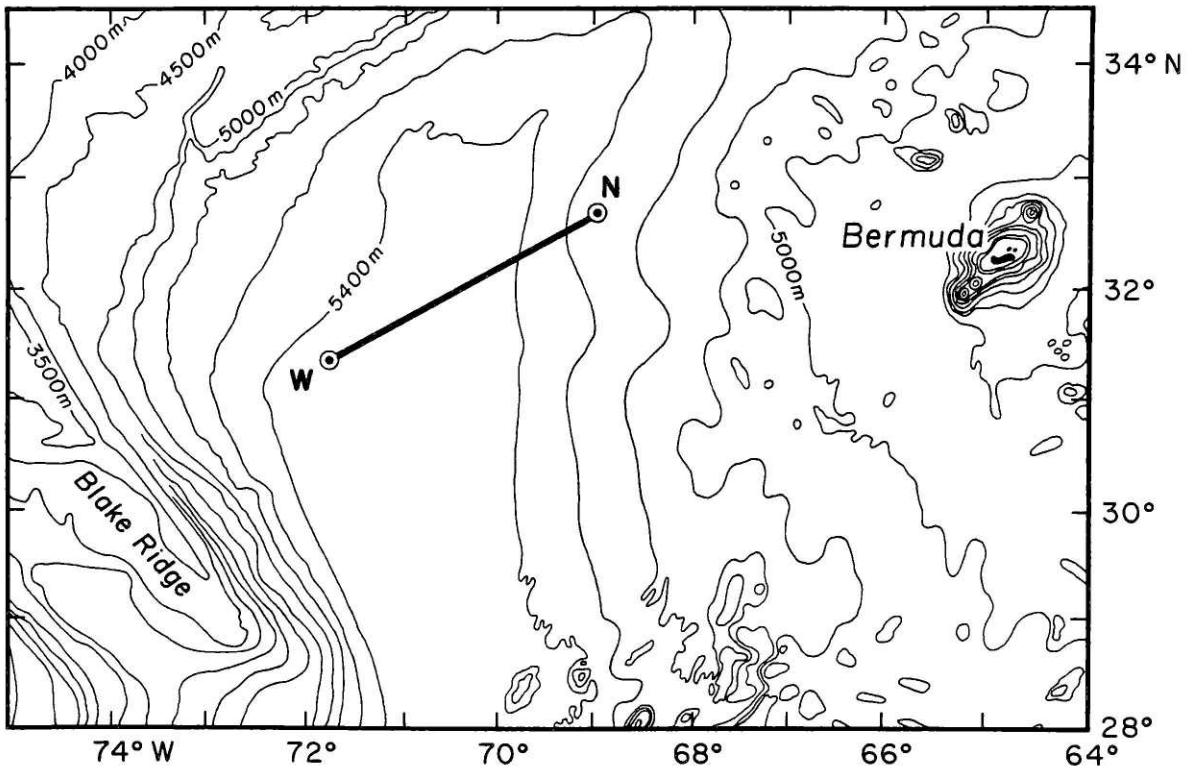

Figure 3.1. Plan view of the 1983 Reciprocal Transmission Experiment, reproduced from Howe [*1986*].

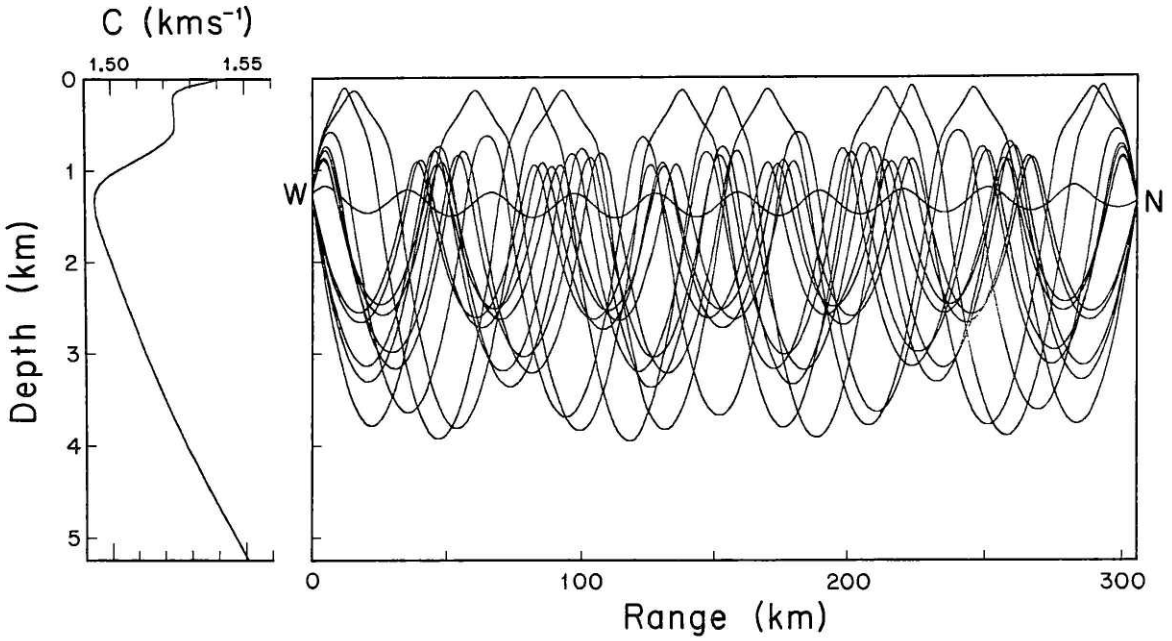

Figure 3.2. Reference sound speed profile (left) and corresponding ray traces (right), reproduced from Howe [*1986*].

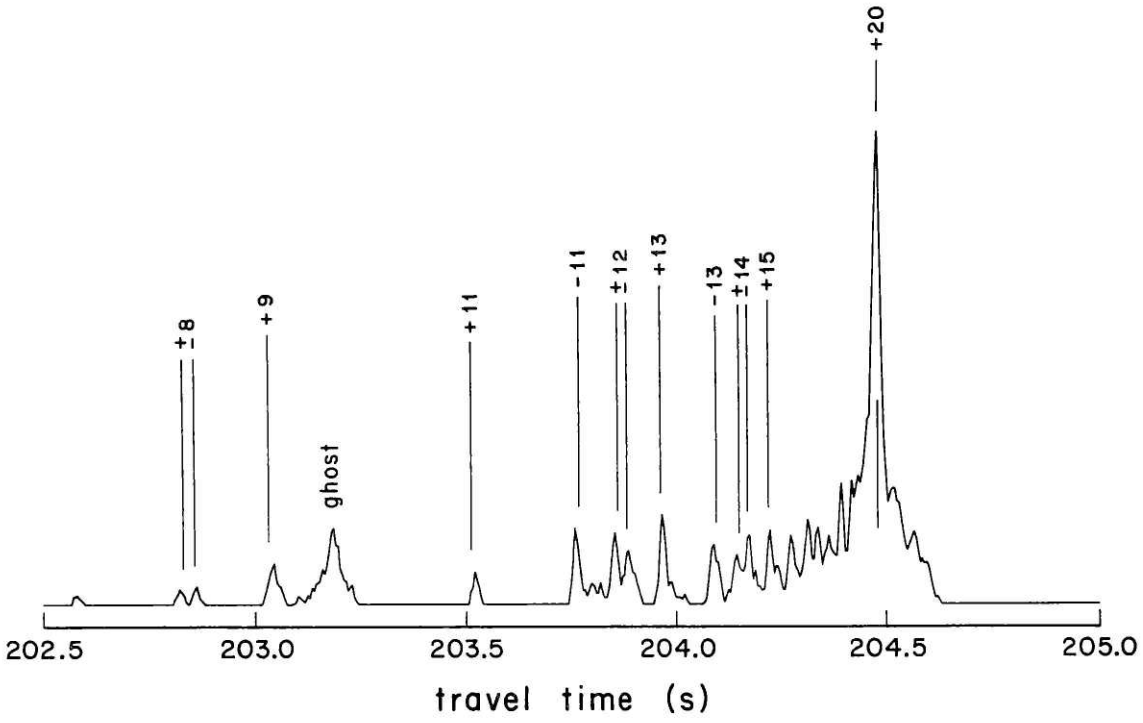

Figure 3.3. The measured arrival pattern, with the 13 resolved rays indicated by their identifier. The identifier is the number of ray turning points. The sign indicates a positive or negative launch angle. The ghost arrival is associated with equipment non-linearity.

measured arrival pattern -- plotted as amplitude, which is proportional to the acoustic pressure measured by a hydrophone, versus travel time. For the purposes of tomographic inversion, the 13 resolved ray arrival times had to be corrected for mooring motion and clock drift. As can be seen in Figure 3.3 (and more clearly in Figure 3.4), the rays tend to come in groups of four -- the four rays with the same number of lower turning points -- that become more crowded toward the end of the arrivals.

The three data sets -- acoustic, XBT, and historical -- were combined to give a range-dependent sound-speed field, C(x,z), and a source-receiver distance such that the measured arrival times are consistent with the prediction of range-dependent ray theory [*Howe, 1986*]. (This sound speed field differed in a small but acceptable way from the field that would have been constructed using only the oceanographic data.) Figure 3.3 also shows the ray theory calculation of the arrival times through this C(x,z).

Figure 3.4 displays the results of the WKBJ theory prediction of the arrival time pattern for the range-averaged C(z). The WKBJ program [*Brown, 1981*] takes a few minutes to run on a PRIME 750 (a large minicomputer). It agrees well with the results of ray theory, within a millisecond for most rays. WKBJ theory is not reliable for axial rays because the final arrival is in general made up of a great many interfering groups of axial rays. Yet only the first few normal modes make up the final arrival. Therefore, it was originally thought that a calculation making use of normal

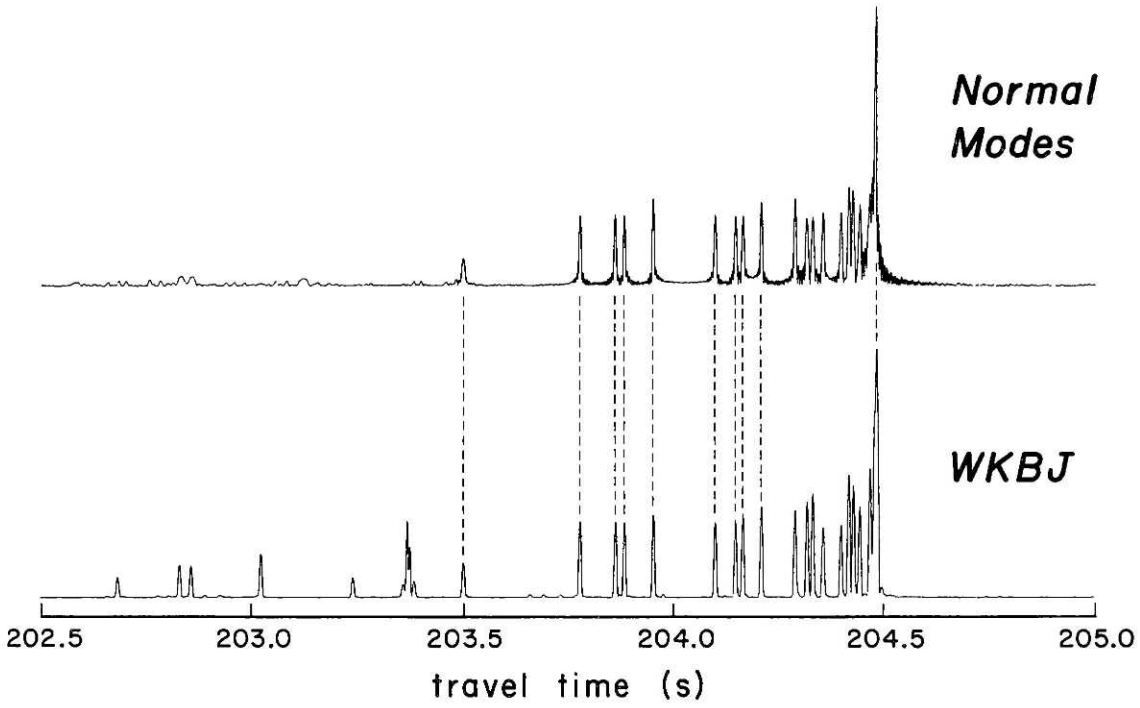

Figure 3.4. Comparison of the arrival patterns predicted using normal mode theory (top) and WKBJ theory (bottom) for the range independent sound speed profile of Figure 3.2. The peaks connected by the dashed lines indicate 10 of the 13 resolved rays. The 250 modes used in the calculation of the top sonogram are insufficient to describe the earliest ray arrivals.

modes might yield some improvement in the prediction of the amplitude and arrival time for the final acoustic arrivals.

The ocean in the region of interest is a smoothly varying waveguide with depth, and so it is well suited to the normal mode analysis described earlier. The result of running the modal program with the range-averaged profile for 250 modes is also shown in Figure 3.4. It took about 3 hours to do this calculation on the same PRIME 750. As can be seen, the complete arrival time pattern was not calculated. The highest modes sample the deep (and shallow) ocean where the sound speed is greatest. Like the deep (and shallow) turning rays, these high modes arrive first. In the calculation done here, 250 modes are insufficient for the earliest arrivals.

There are several different sets of arrival times to compare. There are the arrival times predicted for the range-averaged or range-independent (RI) profile using 1) RI-WKBJ theory, 2) RI-ray theory, and 3) -- RI normal mode theory. As already indicated, RI-WKBJ and RI-ray theory are in good agreement. In addition, there are the arrival times predicted for the range-dependent (RD) profile using Case 4 -- RD-ray theory and Case 5 -- RD (adiabatic) mode theory. Finally there are the measured arrival times, the data, themselves. As has been noted, the range-dependent field was chosen so that RD-ray theory was consistent with the data.

3.1 Range-Independent Mode Predictions

As can be seen in Figure 3.4, the RI-mode calculation is in excellent agreement with the RI-WKBJ approximation. Table 1 compares the arrival time for 21 peaks, including the final arrival. The standard deviation of the difference between the two cases is under 1 millisecond. The relative amplitude of the peaks in the two cases is also in good agreement, even in the case of the final arrival.

As expected, both RI-WKBJ and RI-mode predictions are in good agreement with the data, but there are significant discrepancies. Table 2 compares 12 resolved ray arrivals of the data with the corresponding predictions from mode theory. For several rays there are approximately 10-millisecond discrepancies between the data and the RI-mode prediction. Another difference is that the relative amplitude of the final arrival to the previous arrivals is almost twice as large in the data as it is in either the RI-mode or RI-WKBJ case.

These discrepancies are consistent with the range-dependent field, shown in Figure 3.5 as a departure field $\delta C(x,z)$ relative to the reference range-averaged field of Figure 3.2. In the range-dependent case, the RD-ray theory prediction, by design, agrees well with the data, as shown in Figure 3.3. In the modal case, we have used the linear adiabatic approximation as a first attempt at estimating the effects of range dependence.

TABLE 1

Comparison of MODE and WKBJ arrival times for the DAY 218 Range-Averaged Profile.
(The Identifier is the number of ray turning points. The sign indicates a positive or negative launch angle.)

IDENTIFIER	WKBJ	MODE	MODE - RAY
+ 8	202.831 sec	202.830 sec	-1 msec
- 8	2.857	2.857	0
+ 9	3.023	3.023	0
+11	3.499	3.500	+1
-11	3.775	3.774	-1
+12	3.858	3.857	-1
-12	3.880	3.879	-1
+13	3.952	3.952	0
-13	4.101	4.101	0
+14	4.150	4.150	0
-14	4.167	4.168	+1
+15	4.211	4.211	0
-15	4.292	4.292	0
+16	4.320	4.320	0
-16	4.334	4.334	0
+17	4.358	4.359	+1
-17	4.401	4.401	0
+18	4.420	4.421	+1
-18	4.431	4.430	-1
+19	4.446	4.447	+1
FINAL	4.484	4.482	-2

TABLE 2

Comparison of range-averaged MODE arrival times
with the measurements for DAY 218

IDENTIFIER	MEASURED	MODE	MODE - MEASURED
+ 8	202.827 s	202.830 s	+ 3 ms
+ 9	3.034	3.023	-11
+11	3.513	3.500	-13
-11	3.765	3.774	+ 9
+12	3.855	3.857	+ 2
-12	3.880	3.879	- 1
+13	3.963	3.952	-11
-13	4.090	4.101	+11
+14	4.150	4.150	0
-14	4.169	4.168	- 1
+15	4.222	4.211	-11
+20	4.480	4.482	+ 2

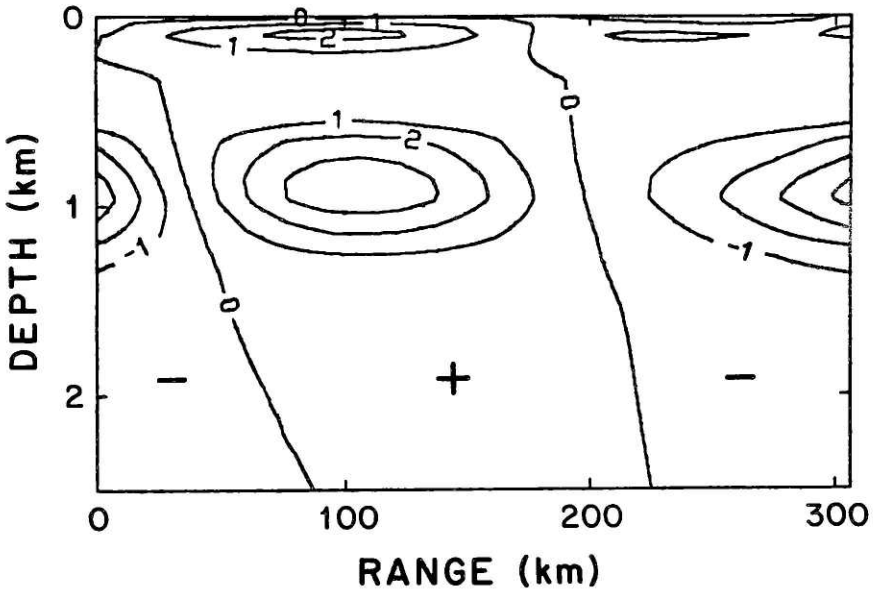

Figure 3.5. The range dependent sound speed field, expressed as a departure field relative to the reference range-averaged field of Figure 3.2, reproduced from Howe [*1986*].

3.2 Range Dependent Mode Predictions

Desaubies et al [*1986*] have examined the limits of the adiabatic approximation and found that it can give adequate predictions of the modal pressure field and arrival times for a typical mesoscale eddy, a geometry similar to the one used in the 1983 experiment, and a frequency of hundreds of Hertz. Since the range-dependence of this experiment, shown in Figure 3.5, is not extreme, the adiabatic approximation seems likely to account for at least some of the discrepancy between the range-averaged and range-dependent travel times and amplitudes.

In the adiabatic approximation, coupling between the modes is neglected, but the local acoustic wavefunctions are retained. In the linear adiabatic approximation, the adiabatic horizontal wave number is the same as that calculated in the range-averaged case, but as described in the previous chapter, the excitations are calculated locally. That is, the excitations are calculated in the profiles of the source and receiver, rather than the range-averaged profile.

The result of correcting the modal amplitudes by calculating them locally is shown in Figure 3.6. The measured arrival pattern and the RD ray theory arrival times are displayed in that figure to show the improved agreement. Table 3 gives a comparison of travel times between the data and RD-mode theory; the

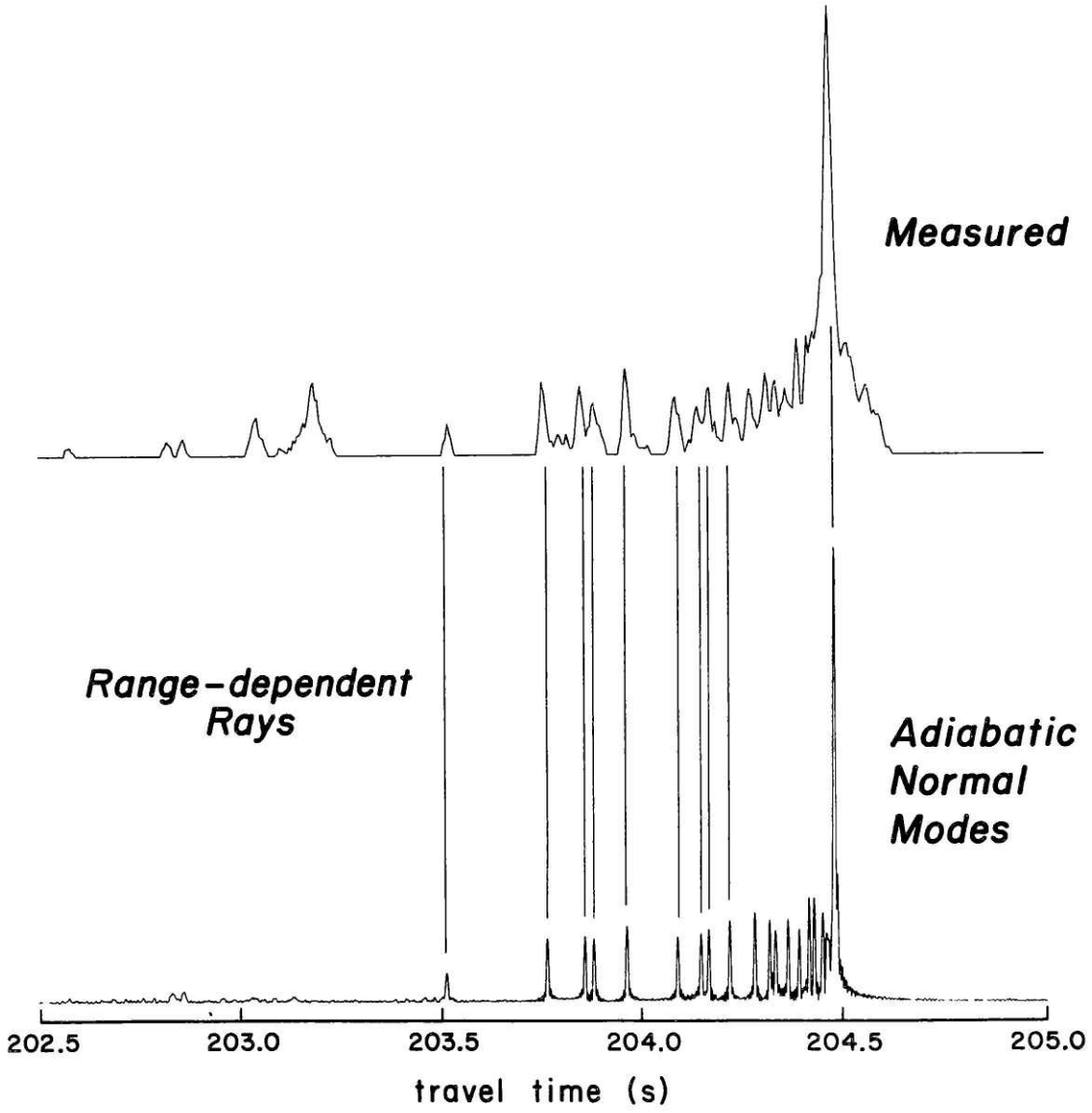

Figure 3.6. Comparison of measured arrival pattern (top) with the arrival patterns predicted using adiabatic normal mode theory (bottom) and range dependent ray theory (lines).

TABLE 3

Comparison of range-dependent MODE arrival times with the measurements for DAY 218.

IDENT.	MEASURED	MODE	Range-Dependent MODE-MEAS	(From Table 2) Range-Indep. MODE-MEAS
+11	203.513 s	203.512 s	-1 ms	-13 ms
-11	3.765	3.763	-2	+ 9
+12	3.855	3.856	+1	+ 2
-12	3.880	3.880	0	- 1
+13	3.963	3.963	0	-11
-13	4.090	4.091	+1	+11
+14	4.150	4.149	-1	0
-14	4.169	4.169	0	- 1
+15	4.222	4.221	-1	-11
+20	4.480	4.481	+1	+ 2

travel-time discrepancy caused by range dependence has largely disappeared. A comparison of the RD-mode result and the data indicates that the amplitude discrepancies have also largely vanished.

4. THE GREENLAND SEA

The second application of normal mode theory is sound propagation in the Greenland Sea. The Greenland Sea is of special interest because it is the source of deep cold-water masses that affect the circulation of the entire ocean.

The Greenland Sea, which lies between Greenland and Norway around 75^0 N and 0^0 W, is the site of a proposed 1988 tomography experiment. Because the Greenland Sea lies so far north, the vertical temperature structure is nearly adiabatic, except near the surface. For this reason, the density is relatively uniform with depth, and the water column is near neutral stability, especially in the winter. Although the exact mechanism for the formation of deep cold water is not agreed upon, it is thought to be due to relatively small temperature and salinity perturbations that cause convective overturning. These perturbations can be difficult to observe by standard spot measurements, but may be resolvable using tomographic techniques.

In the purely adiabatic case, the density varies only with pressure, and the sound speed increases nearly linearly with depth z -- the actual variation is proportional to $\exp[-az]$, but a is about 0.01/km so the linear term dominates in the expansion of

the exponential. (For the Greenland Sea discussion, "adiabatic" will be used solely to refer to nearly linearly increasing range-independent sound-speed profiles and not to the range-dependent approximation discussed earlier.) The depth dependence of typical modes for an adiabatic sound-speed profile were given in Figure 2.2. These modes are very close to Airy functions.

Figure 4.1 shows typical ray paths for an adiabatic profile. The vertical scale is exaggerated; the ray paths are in fact nearly arcs of circles. With increasing distance between source and receiver, the number of rays that reach a receiving point at a given depth increases steadily. Ray optics and WKBJ theory fail as late, shallow arrivals become so crowded that the time interval between arrivals is comparable to the acoustic wave period. In the geometry considered here -- 300 kilometer range, source (250 Hz) and receiver at 200 meters -- ray theory begins to break down for rays with turning points above about 500 meters.

Figure 4.2 shows a typical historical winter profile (March 18, 1982) derived from in situ tempertature and salinity data. It is close to the adiabatic profile and the ray paths, especially for the deep, early rays, are similar to those shown in Figure 4.1. The acoustic arrival pattern for this profile calculated using WKBJ theory is shown in Figure 4.3. The rays still come in groups of four, but with the source and receiver at the same depth, 2 of the rays arrive at the same time, creating the tripartite structure in

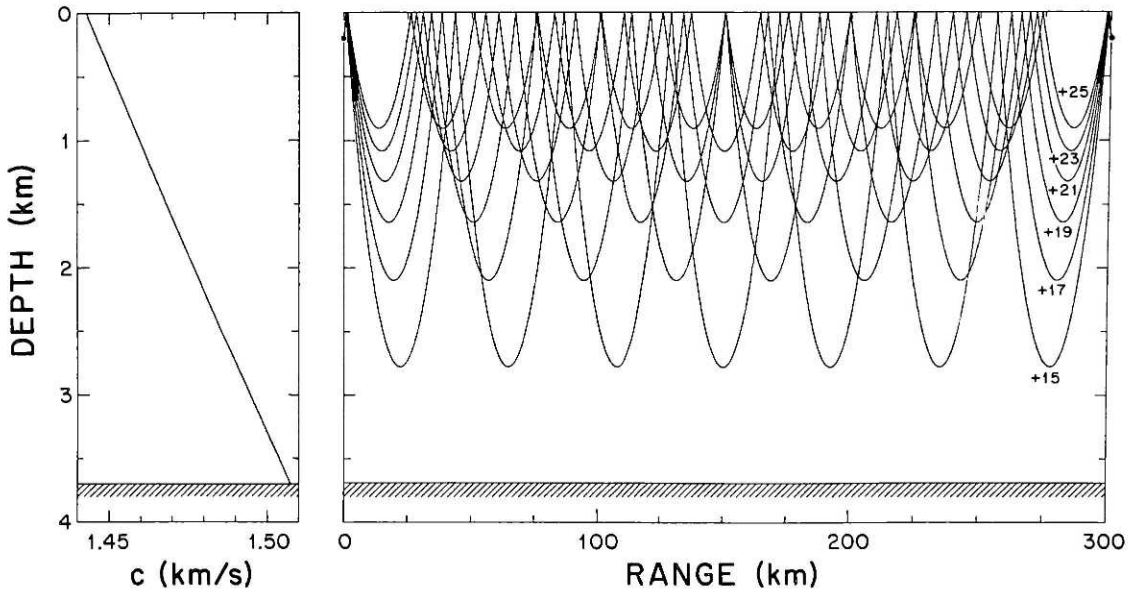

Figure 4.1. The adiabatic sound speed profile (left) and 6 ray traces (right). Source and receiver are at 200 meters.

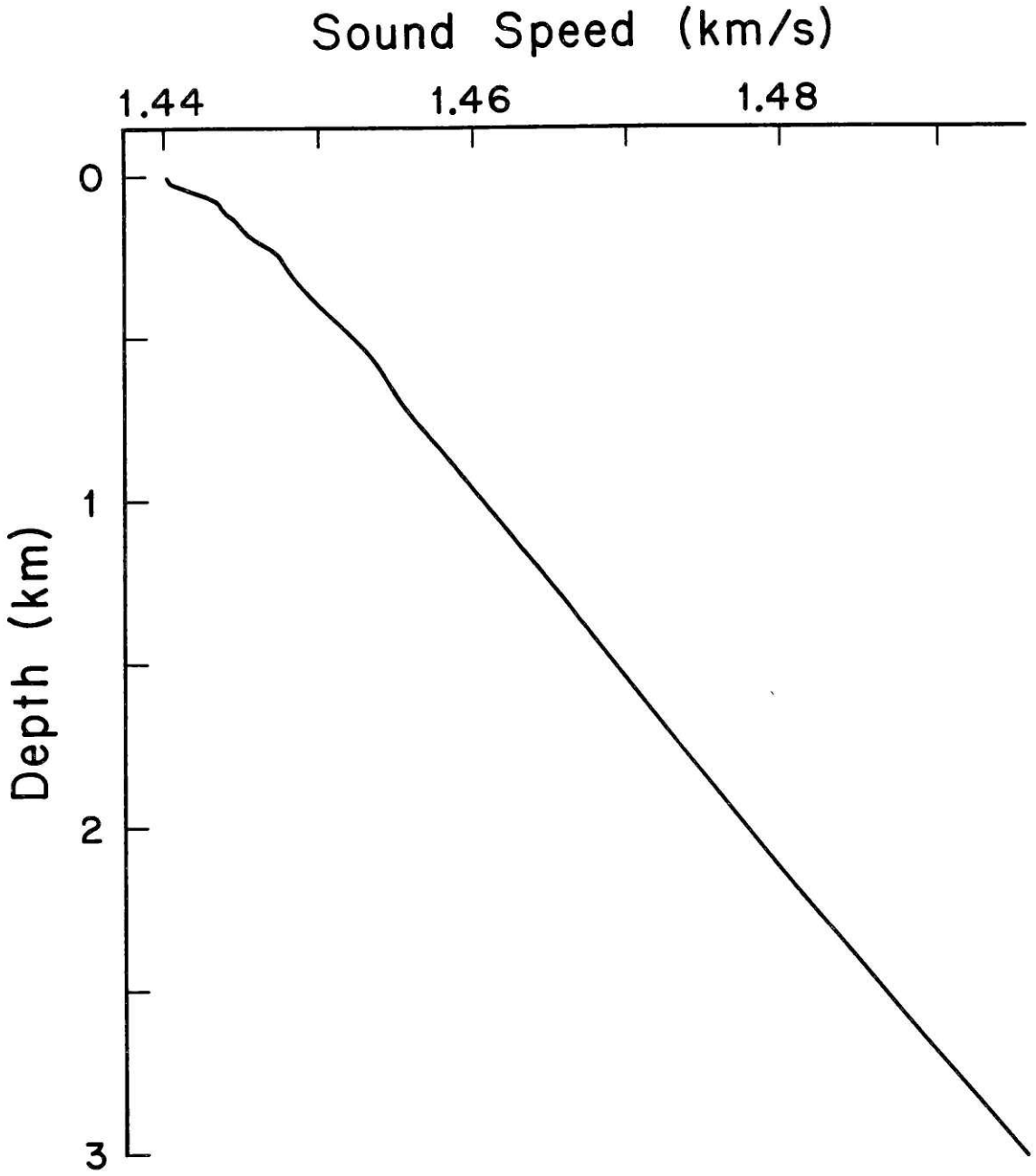

Figure 4.2. Historical Greenland Sea sound speed profile from March 18, 1982.

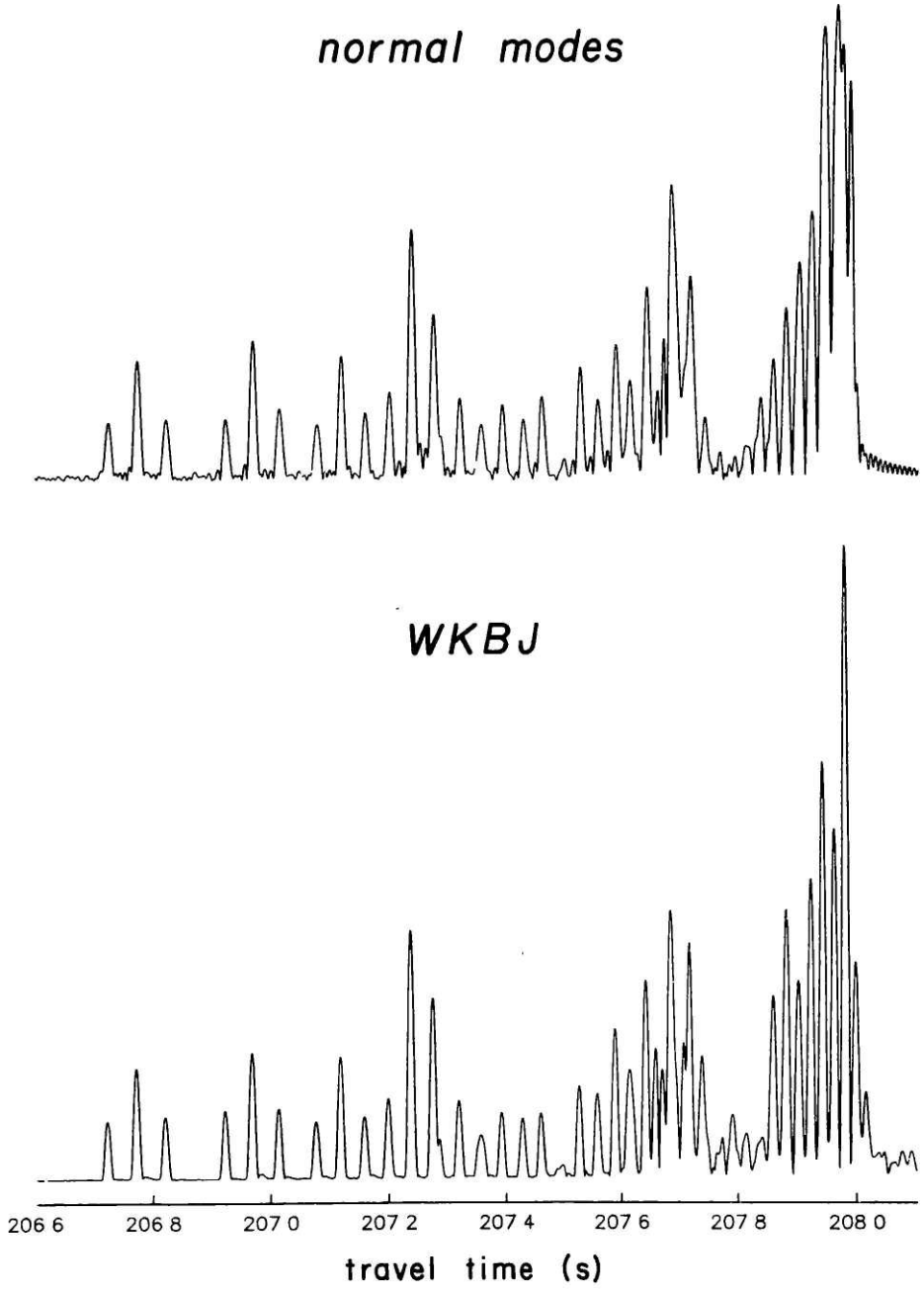

Figure 4.3. A comparison of the arrival patterns predicted using normal mode theory (top) and WKBJ theory (bottom) for the March 18, 1982 sound speed profile of Figure 4.2.

the early arrivals of Figure 4.3. The crowding of the late, shallow ray arrivals can be clearly seen. Figure 4.3 also displays the normal mode calculation for the same winter profile. WKBJ and normal mode theory are in very good agreement for the early arrivals, but the shallow, late arrivals are inadequately described by the WKBJ approximation. WKBJ theory distorts the shape, amplitude, and arrival time of the final arrivals. This distortion extends over the final half second and is far greater than was the case for the mid-latitude profile examined in Chapter Three. Moreover, the identification of distinct rays -- which is crucial for tomographic ray inversions -- becomes increasingly difficult in the final second of the arrival pattern.

In Figure 4.3, the large final arrival is comprised of a great many interfering rays, which is why geometric optics breaks down, but it is made up of only 2 or 3 modes. This is in contrast to the early arrivals, which are well described by a few rays, but which are comprised of hundreds of modes. Each well-defined early ray arrival is made up of more than a dozen modes. This is a facet of the idea that a ray is a locus at which modes are in phase and a mode is a locus at which rays are in phase.

For these reasons, Felsen [*1981*] suggests optimizing computational efficiency with a hybrid calculation that uses a few rays to describe the early arrivals and a few modes to describe the late arrivals. In this thesis, the computational speed of the eigenvalue-isolation algorithm allows most of the analysis to be

carried out exclusively with normal modes. For instance, the final second of the modal arrival pattern in Figure 4.3, which is composed of about 30 modes, can be calculated in a few minutes on the Prime 750, which is comparable to the speed of the WKBJ program. It is only in the tomographic inversions described in the next chapter that ray theory will again become important.

4.1 The Ice Layer

Much of the Greenland Sea is covered with ice during the winter. Although the low vertical stability of the water in the region inhibits ice formation [*Swift, 1986*], this ice layer can be 10 centimeters thick or more. It was originally thought that this ice layer could measurably effect long-range sound propagation. For this reason, the ice model described in Section 2.4 was developed.

In applying this model, values had to be chosen for the the density of ice ρ_1, the compressional velocity of sound in ice α, and the shear velocity of sound in ice β. Unfortunately, in situ measurements of the sound velocities in ice vary from experiment to experiment and with theoretical estimates [*Stein, 1986*]. I have chosen to use the values selected by Stein, who takes into account both theory and data. He uses α=3500 m/s, β=1800 m/s, and ρ_1=910 kg/m^3.

To test the ice layer model, the mode locked onto the ice-water interface was calculated for a wide range of frequency-thickness

(f·d) products. This mode has a phase velocity below the speed of sound in either water or ice, so the amplitude of the mode has a maximum on the interface and decreases with distance on either side of the interface. At low frequencies, this mode is a flexural or bending mode, and at high frequencies, it asymptotically approaches the Stonely wave along the interface. The phase and group velocities of this mode were calculated for a wide range of frequencies and ice thicknesses. These results are in excellent agreement with theoretical predictions [*Stein, 1986,* and *Ewing et al, 1957*]. The asymptotic value of the velocity of the Stonely mode calculated by the normal mode program, 1206.6795 meter/second is also in complete agreement with theoretical predictions [*Ewing et al, 1957*].

Because this mode is purely exponential in water, it is not significantly excited for acoustic sources deeper than 10 meters. But even if the interface mode were excited, it would be rapidly attenuated. The acoustic modes that are locked entirely into the ice layer are also poorly excited by acoustic sources in water, and they are also rapidly attenuated. At the frequencies and ice thicknesses of interest, all of the ice modes and interface modes are attenuated at a rate of more than 10 dB/km [*Stein, 1986*]. Because only long-range propagation over hundreds of kilometers is considered here, these modes have been neglected in the calculation of the acoustic arrival pattern. Therefore, only the modes that are locked in the ocean -- and that are purely

exponentially decaying in the ice -- need be included in the calculation, and so the formalism developed in Chapter Two can be used.

To test the effect of ice on normal mode propagation, a 1-meter ice layer was placed on the winter profile used above. Figure 4.4 compares the acoustic arrival pattern calculated with and without the ice layer. The difference between the two is very small. The amplitude and arrival time of a few peaks have been changed slightly, but not significantly. The character of the individual modes has not been greatly altered. This would not occur until the thickness of the ice approached a vertical wavelength. Mode 0, which has its maximum closest to the surface and is usually the mode most affected by the ice layer, is not significantly altered until the ice layer approaches a thickness of 5 meters.

With or without the ice layer, all of the modes have zeroes in pressure at the surface. Because the modes that are locked in the ocean waveguide are exponential in the ice, the pressure decays toward zero much more rapidly in the ice than in the water. For this reason, the ice layer does little more than shift the displacement fields of the modes up a distance that is nearly equal to the ice thickness. Since the vertical sound speed profile does not change much over the scale of one meter, shifting the modes one meter has little effect on them. Since all of the modes are shifted about the same amount, this shifting usually has even

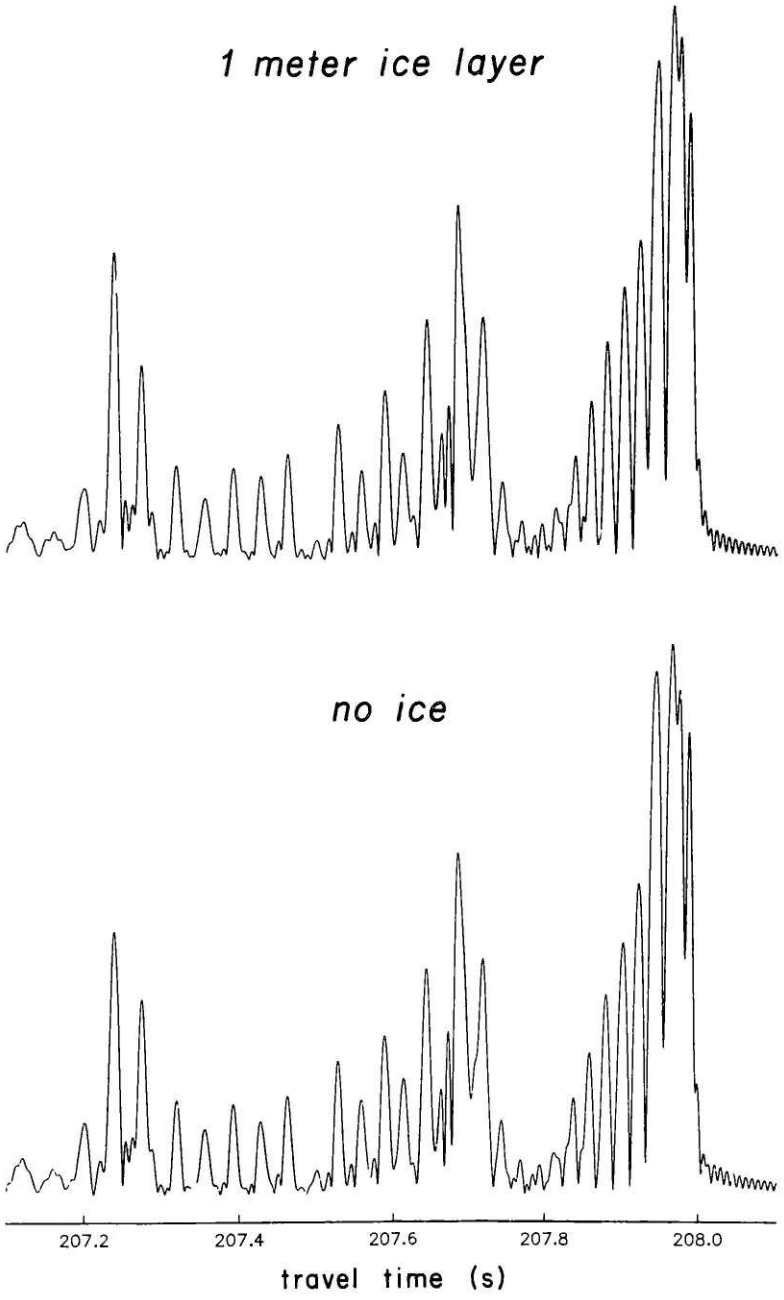

Figure 4.4. A comparison of predicted normal mode arrival patterns calculated with (top) and without (bottom) a one-meter ice layer for the March 18, 1982 sound speed profile of Figure 4.2.

less effect on the acoustic arrival pattern, which is composed of the interference of neighboring modes.

The decision to put the ice layer directly on top of the winter profile has maximized the effect of the ice. If, for instance, the ice had been placed 9/10 of the way into the water (which would be modeled by neglecting the top 0.9 meters of the winter sound-speed profile), the individual modes would have been shifted up by only about 0.1 meters. In this case, the effect of the ice on the arrival pattern would be significantly reduced. Since the thickness of the ice in the Greenland Sea is probably much less than 1 meter most of the time, the effect of ice on sound propagation can be neglected.

5. TOMOGRAPHIC INVERSIONS

The key process to be studied in the Greenland Sea is the onset of adiabaticity involved in deep cold water formation during the winter. A central question is whether this process can be observed acoustically. For this reason, the synthetic sound speed profile to be considered in this chapter is an adiabatic profile. The "data" in this synthetic experiment is the acoustic arrival pattern calculated using the adiabatic profile.

In an actual tomographic experiment, in situ temperature and salinity data taken at the beginning of the experiment would be used to determine a starting sound speed model for the inverse procedure. For the purposes of the synthetic experiments discussed in this chapter, the starting sound speed model will be generated by averaging 25 sound speed profiles calculated from historical Greenland Sea temperature and salinity data taken from mid-March to early May between the years 1958 and 1982. This average profile, $\alpha_0(z)$, is displayed in Figure 5.1 as a difference from the adiabatic profile, $\alpha(z)$. As can be seen, the difference, $\delta\alpha = \alpha(z)-\alpha_0(z)$ is of the order of 0.5 meters per second. This is comparable to the difference that would be found if the starting model were based on temperature and salinity data taken at the

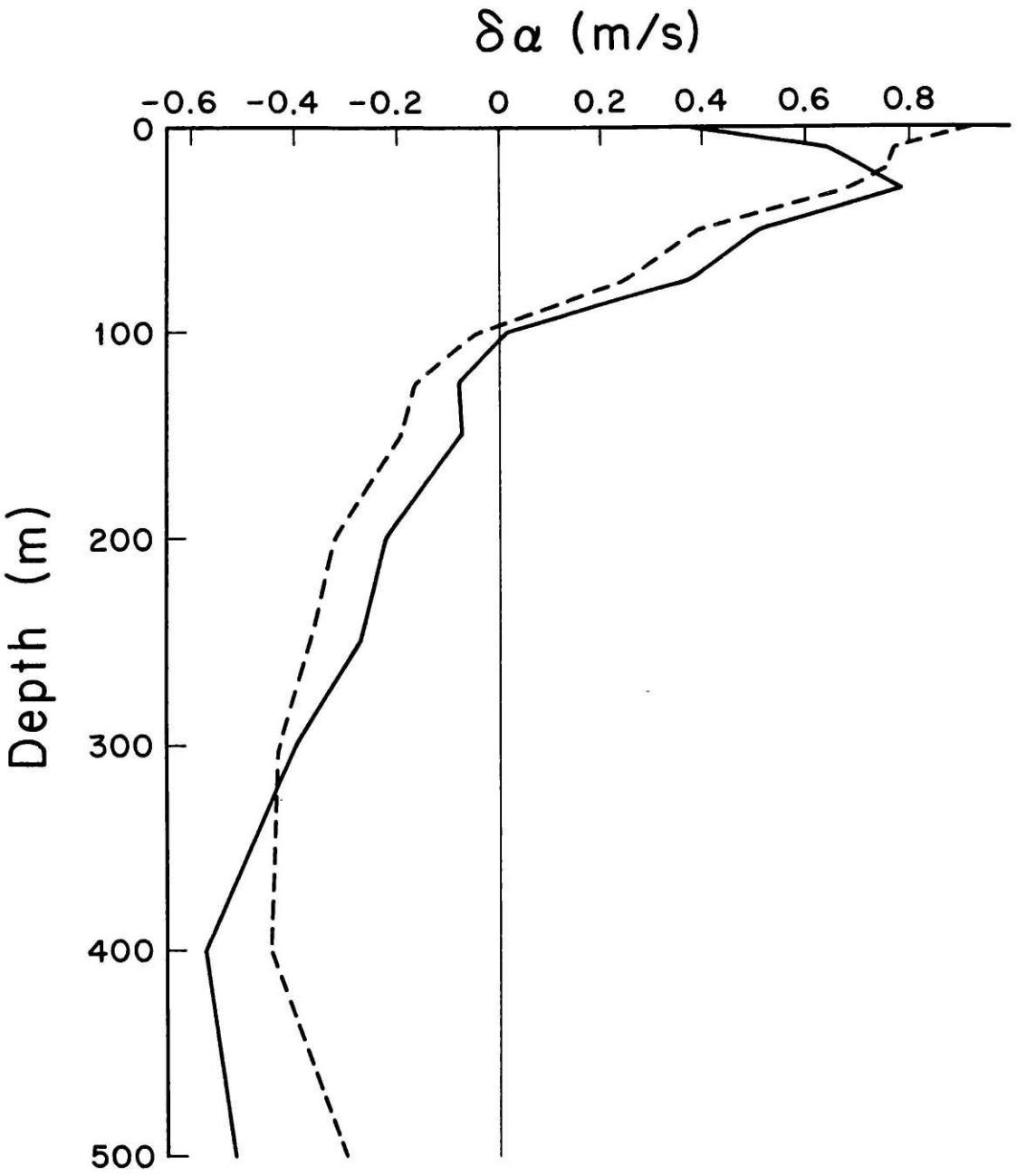

Figure 5.1. The difference $\delta\alpha(z)$ between the adiabatic profile and the average of 25 historical profiles (solid curve) compared with -0.4 times $E_2(z)$, the second empirical orthogonal function (dashed curve).

beginning of the experiment, and so this average profile is a reasonable starting model for the synthetic experiment.

The statistical variation between each of the 25 profiles and the average profile was also examined. It turns out that 90% of the variation in these 25 profiles can be accounted for by two orthogonal functions, called empirical orthogonal functions (EOFs), shown in Figure 5.2. In other words, if the first EOF is written as $E_1(z)$, and the second EOF is written as $E_2(z)$, and the average of the 25 profiles is written as $\alpha_0(z)$, then it is a reasonable first approximation to write each of the 25 profiles, $\alpha_i(z)$ -- i = 1 to 25 -- as

$$\alpha_i(z) = \alpha_0(z) + a_{1i}E_1(z) + a_{2i}E_2(z)$$

While this decomposition scheme does not account for some 10% of the variability of the profiles, it does allow the profiles to be described by two numbers, a_1 and a_2, the amplitudes of the two EOFs. If the profile to be decomposed is the adiabatic profile $\alpha(z)$, then a_1 is approximately -0.04 and a_2 is approximately -0.40. This means that while the first EOF accounts for 75% of the variation among the 25 historical profiles, it accounts for very little of the difference between the adiabatic profile and the average profile. On the other hand, the second of these two EOFs is very similar to this difference, as shown in Figure 5.1. This suggests that a significant fraction of the 25 profiles have an

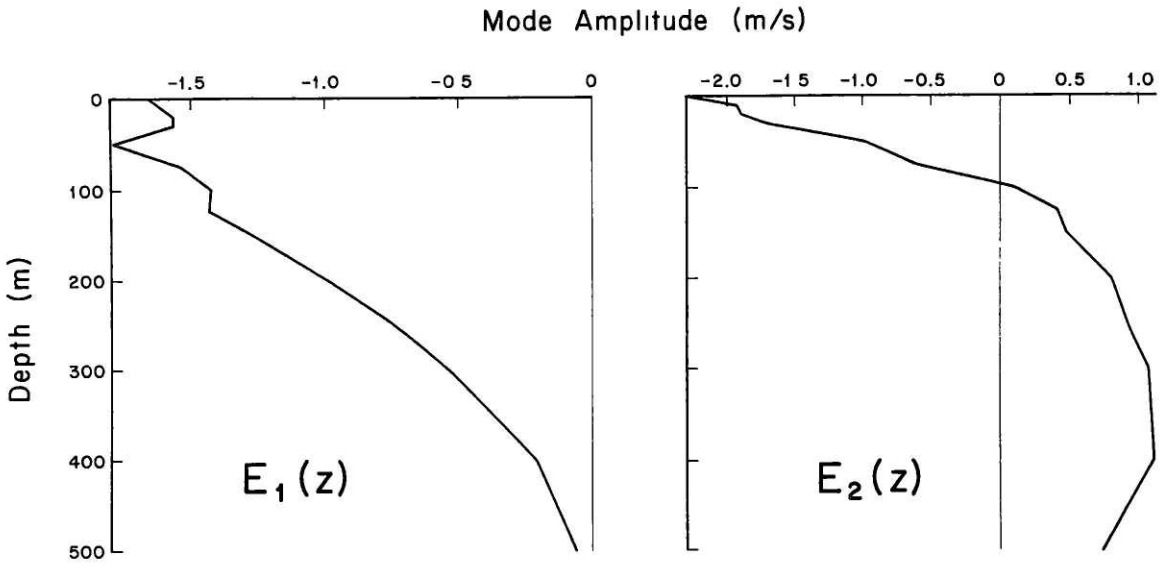

Figure 5.2. The first two empirical orthogonal functions, $E_1(z)$ and $E_2(z)$, calculated using 25 historical Greenland Sea sound speed profiles.

adiabatic component. It also suggests that the amplitudes of the EOFs are the appropriate quantities to solve for using the inversion techniques described in Chapter Two. If the amplitudes of the two EOFs can be tracked as a function of time, then the onset of adiabicity can be identified with the normally large amplitude of $E_1(z)$ becoming much smaller than the amplitude of the $E_2(z)$.

Although sound-speed data is available from the surface down to below 3000 meters, the EOFs have been calculated down to only 500 meters, for several reasons. First, as seen in Chapter Four, WKBJ and ray theory are adequate to describe sound propagation in the Greenland Sea beneath 500 meters, and they are faster and easier to use than mode theory. Moreover, the Greenland Sea deep water, which extends on average from 420 meters down to the bottom (at about 3000 km), has extremely little variation [*Swift, 1986*]. Therefore, monitoring its change should not be difficult for either WKBJ or ray theory. Above 500 meters, however, neither of these theories is adequate to describe sound propagation. Finally, for most of the proposed deep-water formation mechanisms, much if not most of the formation action takes place above 500 meters [*Swift, 1986*]. For these reasons, normal modes are used exclusively to handle tomographic inversions above 500 meters, while it is assumed that the rest of the water column will be handled by WKBJ and ray theory.

The EOFs, by virtue of their orthogonality, are relatively easy

to distinguish with only a small amount of data (in the form of modal group velocities) if there is information about the ocean where the two EOFs both have significant values and different structures, which occurs above 200 meters. Putting the source and receiver at 200 meters, as before, may not be adequate to the task. The case discussed here considers a source and receiver at 140 meters, a depth chosen because it is near the maximum of the vertical displacement field for the second normal mode in near-adiabatic sound speed profiles. The point is to try to identify the arrival times and therefore the group velocities of the early modes. To help in this identification process, multiple acoustic receivers are considered, and these receivers are placed at depths convenient to observing the first few modes -- 50, 80, 140, 175, 225, and 270 meters. The receiver at 50 meters is at the maximum of the vertical displacement field for mode 0, as can be seen in Figure 2.2. Although it is difficult in practice to have a receiver at 50 meters, it may, as will be shown, be worth the effort. For example, such a string of receivers may make possible the mode isolation or mode filtering scheme described in Chapter Two.

Figure 5.3 shows the "observed" arrival patterns for the adiabatic ocean at the six selected receiver depths. As can be seen, the final arrivals can be observed only by the shallow receivers, strongly suggesting that these arrivals represent the lowest modes. Nevertheless, these arrivals cannot be identified

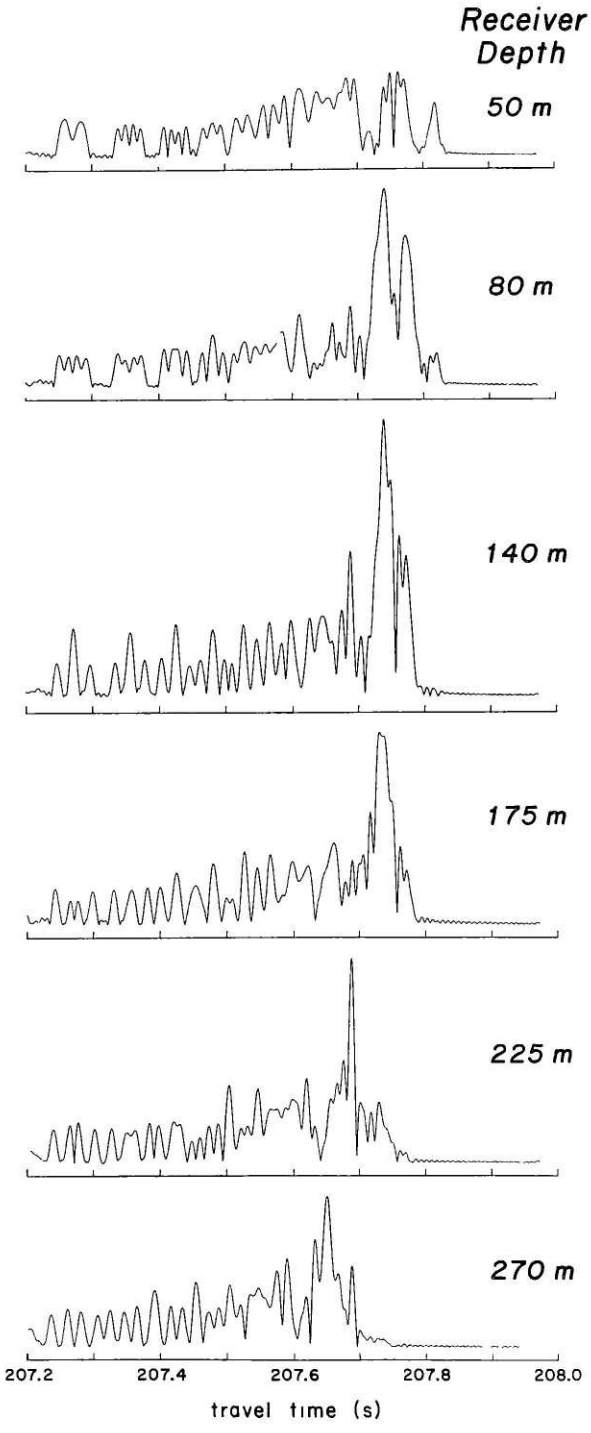

Figure 5.3. The "observed" arrival patterns for an adiabatic ocean with source at 140 meters and receivers at 50 (top), 80, 140, 175, 225, and 270 (bottom) meters.

as particular modes without comparison with the starting model.

Figure 5.4 shows part of the arrival pattern for the average profile (starting model) for the receiver at 140 meters. Since the group velocities of all the modes are explicitly calculated for the starting model, it is known that the large final peak is made up almost entirely of mode 2, and that the smeared out peak that arrives just afterwards is mode 1. Figure 5.4 also shows the arrival pattern for the adiabatic profile (data) for the receiver at 140 meters. The approximate shape of the final arrivals suggests that the large final peak should be identified with mode 2 here also, and that the smaller peak that arrives immediately afterwards should be identified with mode 1. Further support for this view is provided by comparison of the arrival patterns for the other five receivers.

Rather than showing all those other arrival patterns, I will show only the most striking -- the arrival pattern for the receiver at 50 meters, shown in Figure 5.5. Here, the very final arrival in both the average and the adiabatic profile comes in completely separate from the other arrivals, as if it were one of the distinct early ray arrivals. In the case of the average profile, however, it is known that this peak is mode 0, and it certainly seems very reasonable to identify the last peak for the adiabatic profile with mode 0.

For the first iteration of the inversion procedure, three pieces of data are used -- the group velocity differences for modes 0, 1,

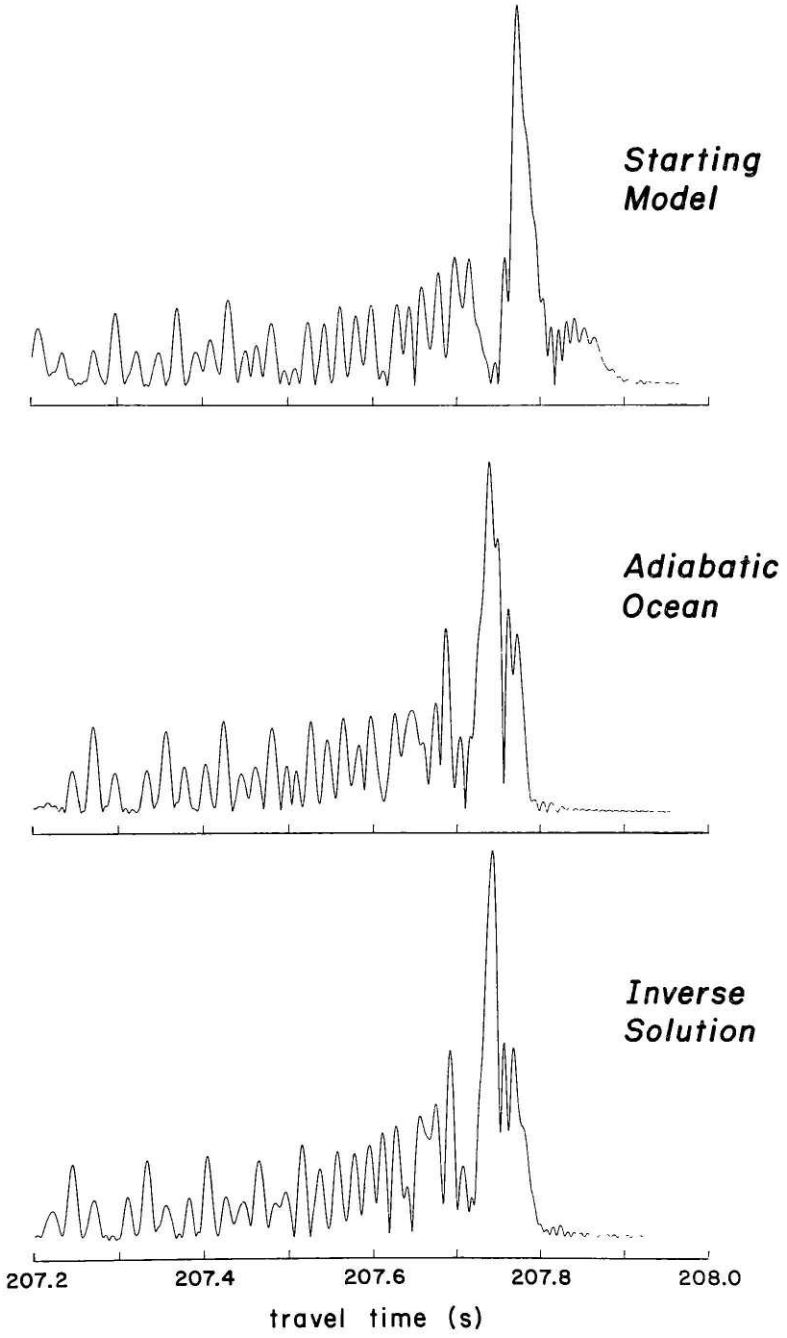

Figure 5.4. The "observed" arrival pattern for an adiabatic ocean (middle) compared with the arrival pattern calculated using the starting model (top) and with the arrival pattern calculated using the inverse solution (bottom). Source and receiver are at 140 meters.

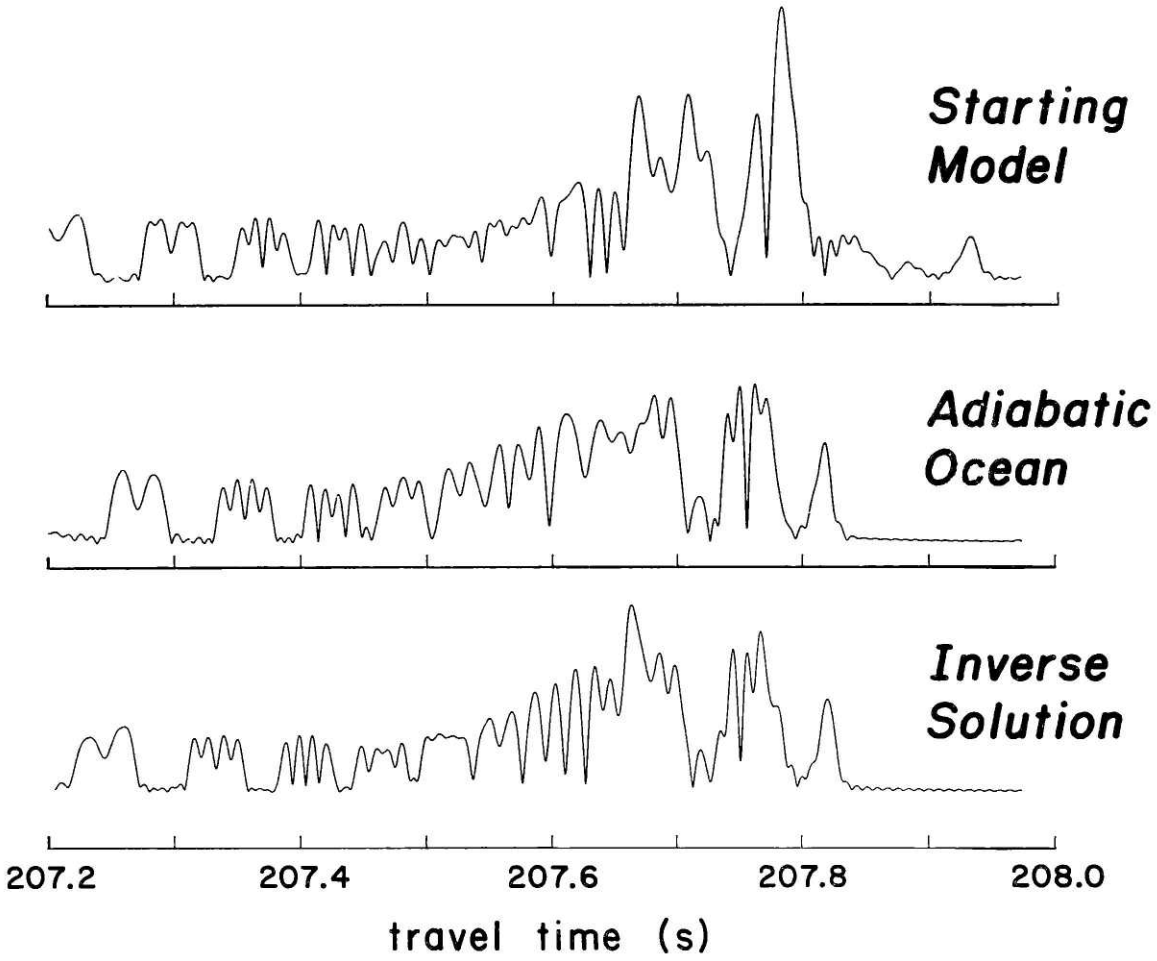

Figure 5.5. Same as Figure 5.4 except the receiver is now at 50 meters.

and 2. The group velocity kernels are then calculated in the starting model. The frequency at which the group velocity kernels are calculated is found by determining the frequency at which the corresponding peak in the arrival pattern occurs. Since the group velocity of each mode as a function of frequency has already been calculated for the starting model, this is easy to do. For mode 2, the large final peak in Figure 5.4 occurs at about 270 Hz. To use this mode as data in the inversion requires two assumptions -- first, that the large peak in the data is mode 2, and second, that it occurs at the same frequency, 270 Hz. For sound speed structures that are significantly dissimilar, as is the case here, even when the first assumption is correct, the second assumption is likely to be incorrect. The errors assigned to the data must take this into account. Being off by 25 Hz can result in 10 millisecond errors, which was approximately the errors used in the first iteration of the group velocity inversion discussed here. The errors assigned to the data are somewhat arbitrary, but this is not a significant problem because the ocean model constructed by the inverse procedure is not particularly sensitive to the assigned errors at this stage.

The inversion procedure can give confidence in the process of associating peaks with modes at a given frequency if it yields an arrival pattern that is closer to the data than the one the starting model yielded. In this case, the inversion yielded a value for a_1 of -0.04 ± 0.05 and for a_2 of -0.38 ± 0.05. These values may be

used to construct a sound speed model of the ocean $\alpha_1(z) = \alpha_0(z) - 0.04E_1(z) - 0.38E_2(z)$. Figures 5.4 and 5.5 also show the arrival patterns calculated with this constructed model of the ocean, referred to here as the inverse solution. It is quite clear that these waveforms are much closer to the corresponding waveforms of the data than the waveforms of the starting model. This strongly suggests that the modal identifications were made correctly and that the inverse solution is closer to the adiabatic profile than the average profile.

The mode isolation or filtering scheme can provide further support for this view. Although the starting model was too different from the adiabatic ocean to use the mode filtering process, the inverse solution is not. The observed waveforms are composed almost exclusively of modes 0 to 4 in the interval from 207.63 seconds on. Using the modal amplitudes from the inverse solution, and the observed arrival patterns in this interval, each of the first five modes of the adiabatic profile was isolated. The arrival times of modes 0, 1, and 2 determined by mode filtering agreed with the arrival times originally assigned to them to within a few milliseconds. In addition, the arrival times of modes 3 and 4, as isolated from the observed data using the mode filtering process, agreed well with the arrival times of modes 3 and 4 calculated from the inverse solution, even though these modes were not used in the inversion process. Figure 5.6 compares mode 4 isolated from the data with mode 4 synthesized

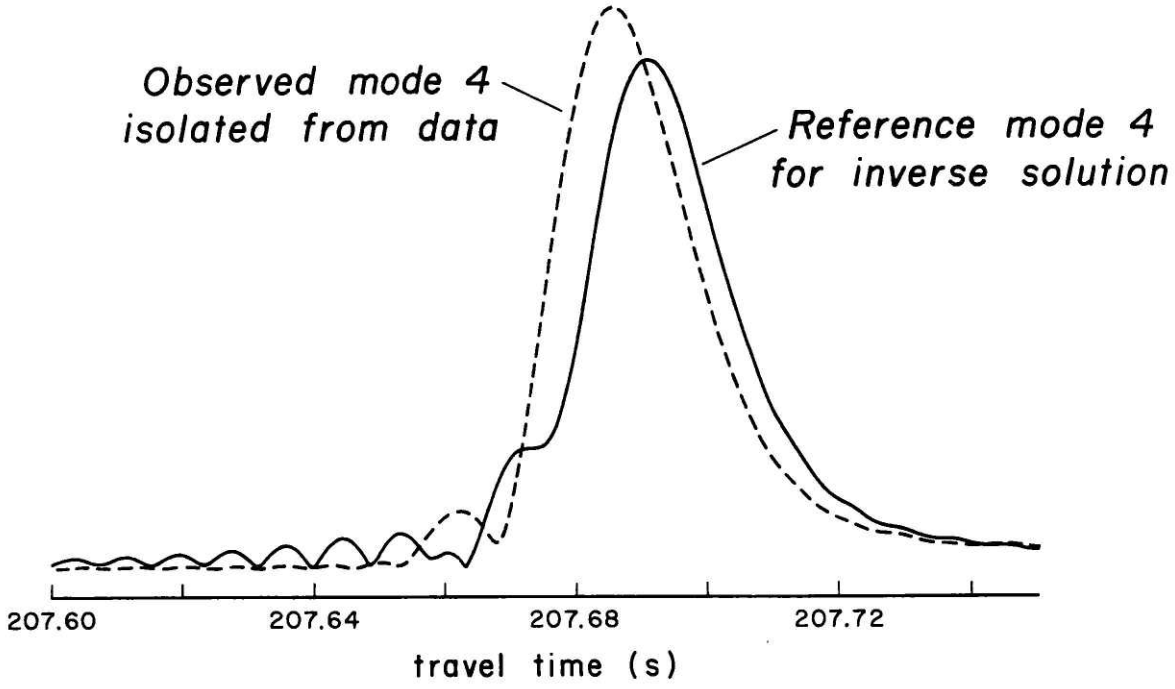

Figure 5.6. Comparison of the arrival pattern of Mode 4 synthesized from the inverse solution (solid curve) with Mode 4 isolated from the data (dashed curve) using the mode filtering technique.

from the inverse solution. The agreement is good enough to suggest that the inverse solution is close to the actual ocean, while the disagreement in arrival time is enough to allow the difference in group velocity to be used as data in the next iteration of the inversion.

In spite of the good agreement between the various waveforms, in an actual experiment it would not be possible to tell if the inverse solution is actually close to the true ocean. In this synthetic experiment, however, it is possible because the "actual" ocean is known. The difference between the inverse solution and the actual ocean (the adiabatic profile) is shown in Figure 5.7 with error bars at selected depths. These error bars represent the error averaged over nearby depths; they are somewhat arbitrary because they are derived from the errors assigned to the data. If this curve, $\alpha(z)-\alpha_1(z)$, were zero everywhere, the inversion procedure would have been completely successful. Here this is not possible, since no values of a_1 and a_2 could provide a perfect fit. That is, the two EOFs do not have enough degrees of freedom to account for all of the difference between the average profile and the adiabatic profile; this difference, which was shown in Figure 5.1, is shown again in Figure 5.7 for comparison.

The fact that the agreement is best from about 30 meters to 300 meters is not surprising considering that the receiver array extends from 50 meters to 270 meters and that only a few early modes were used in the inversion. The top 20 or 30 meters will

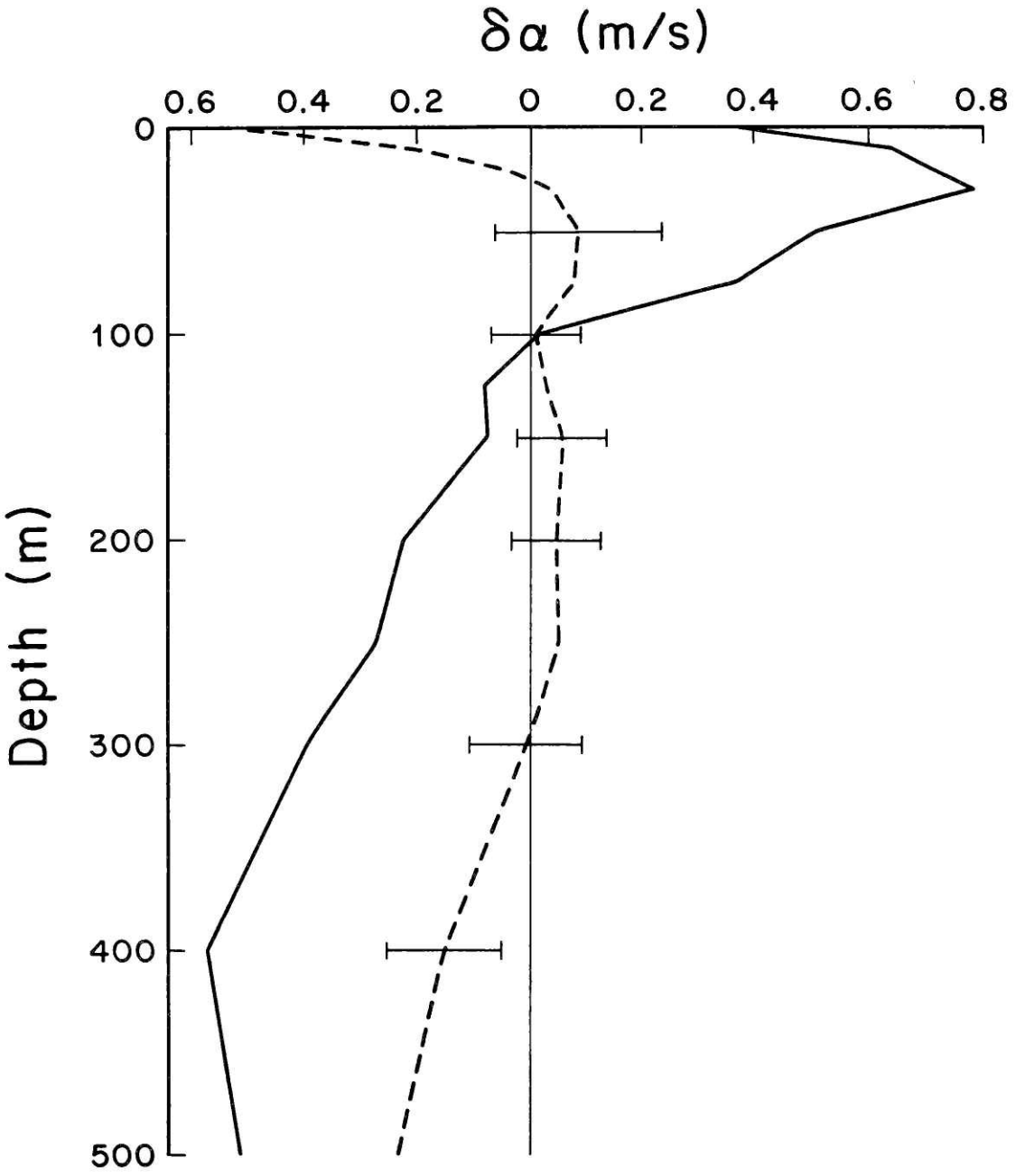

Figure 5.7. The difference between the inverse solution and the assumed adiabatic ocean (dashed curve) compared with the diference $\delta\alpha(z)$ between the adiabatic profile and historical average (solid curve, also shown in Figure 5.1).

never be well resolved with this receiver array; mode 0 can only give an average value of the sound speed for the top 60 meters or so. The identification of higher modes in the next iteration of the group velocity inversion should help the resolution of the ocean structure from 300 to 500 meters. Moreover, in a more sophisticated inversion, one combining modes and rays, the shallow turning rays would provide information about the ocean near 500 meters.

Without the receiver at 50 meters, mode 0 would not be observable in the data, and could not be used in the inversion. In that case the values of a_1 and a_2 determined by the inversion have much larger error bars and, the resolution of the top 100 meters is much worse. In this particular example, the mode isolation scheme is not very dependent on the receiver at 50 meters because mode 0 comes in very distinctly from modes 1, 2, 3, and 4 and so it is possible to isolate an interval of the observed waveforms that consists solely of these four modes. In other cases, where there is more interference among the modes, the absence of this receiver could seriously degrade the mode filtering scheme.

Because the inverse solution $\alpha_1(z)$ is so much closer to the actual ocean $\alpha(z)$ than the average profile $\alpha_0(z)$, $\alpha_1(z)$ makes a much better starting model for a group velocity inversion. Using mode filtering and the arrival patterns at the six receivers, it is possible to identify far more than three modes for the second inversion. Figures 5.4 and 5.5 indicate some of the peaks

identified with modes and used as data in the inversion.

To handle the greater number of degrees of freedom needed to describe the difference between the inverse solution and the adiabatic ocean, the two EOFs were replaced by triangle funcitons at seven selected depths -- 0, 30, 75, 125, 200, 300, 400 meters. These triangle functions are unity at the selected depth, and go to zero at the adjacent depths linearly. This is similar to using layers of constant sound speed, which were described in Chapter Two, but it avoids the discontinuities in sound speed that a layered model creates because a weighted sum of the triangle functions is equivalent to linear interpolation between the selected depths [*Worcester, 1985*]. Since the inverse solution is fairly close to the adiabatic ocean, the exact form of the functions used at this stage of the iteration procedure is not crucial; different sets of functions give similar inverse solutions.

A second inversion was done. This inversion had much more data, and the errors assigned to the data were much smaller, on the order of a few milleseconds. The mode filtering procedure in particular made it possible to determine the group velocity of the early modes with a precision comparable to that found in the measured ray arrival times of the RTE83 experiment [*Howe, 1986*].

Figure 5.8 shows the similarity between the arrival pattern for the adiabatic ocean and the arrival pattern for the second inverse solution, for the receiver at 140 meters. Figure 5.9 compares the difference between the second inverse solution and the adiabatic

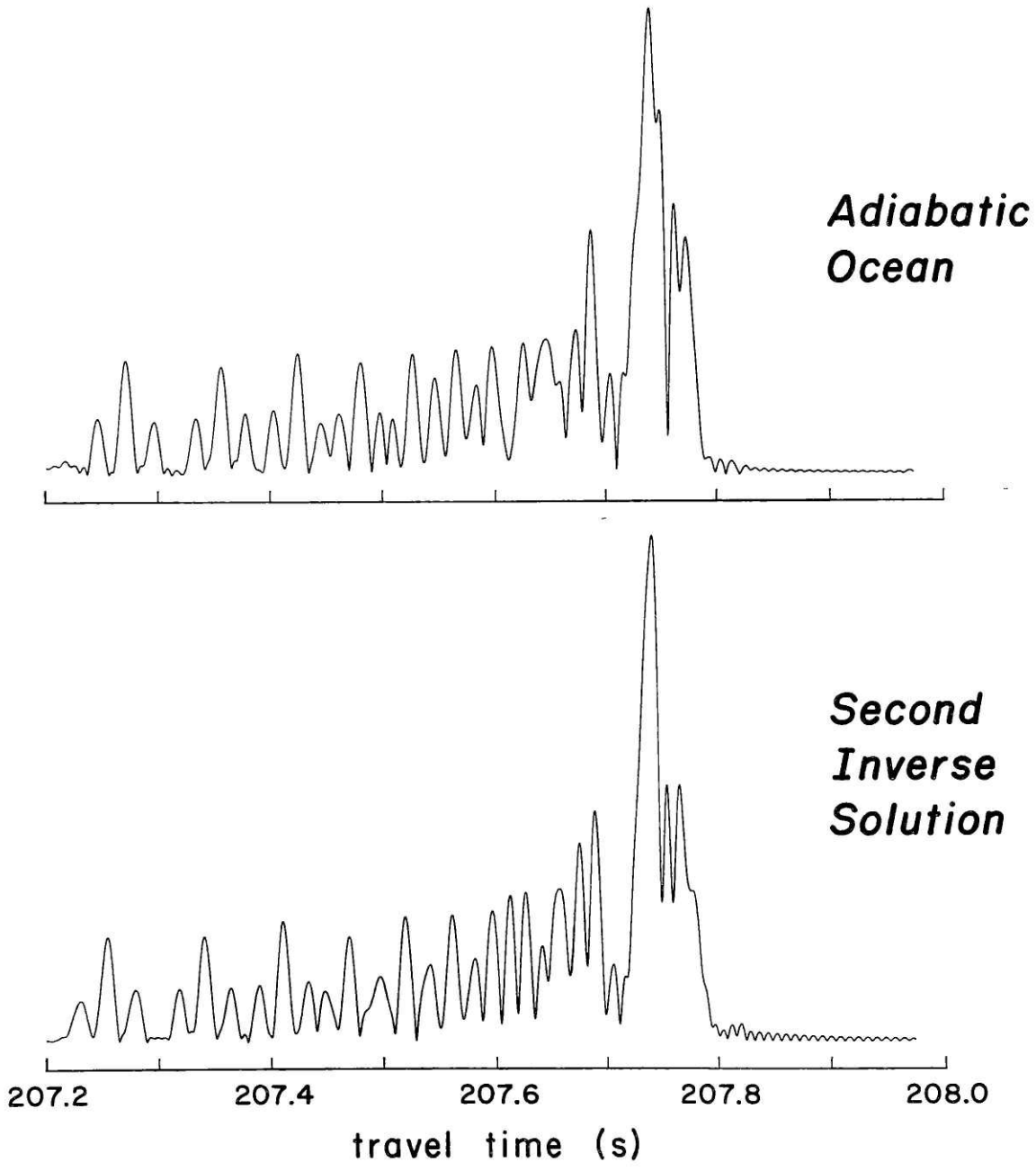

Figure 5.8. The "observed" arrival pattern for an adiabatic ocean (top) compared with the arrival pattern calculated using the second inverse solution (bottom). Source and receiver are at 140 meters.

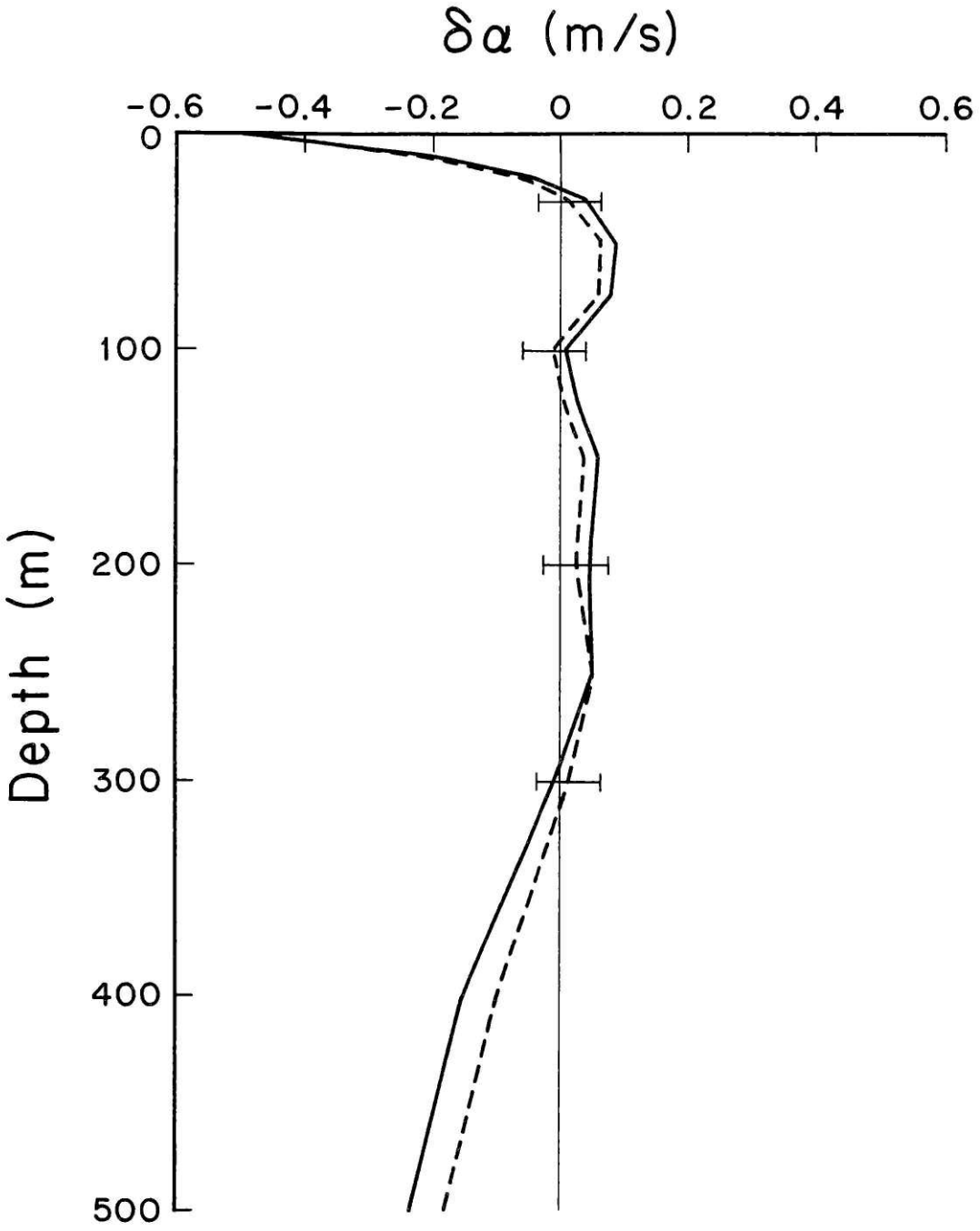

Figure 5.9. The difference between the second inverse solution and the assumed adiabatic ocean (dashed curve) compared with the difference between the first inverse solution and the assumed adiabatic ocean (solid curve).

ocean with the difference between the first inverse solution and the adiabatic ocean (which was also shown in Figure 5.7). As can be seen, there is a slight improvement at almost every depth. Error bars are given at selected depths. From near the surface to about 350 meters, these depth-averaged errors are of the order of 0.02 meters per second, or well under 0.01^{0}C. A true assessment of the errors would require a formal resolution analysis, which is the subject of future work. For the late-arriving low modes, the second inverse solution fits the arrival time data very well, to within 2 or 3 milliseconds. Yet, there is still a 5 to 10 millesecond discrepancy between the early arriving modes identified in the observed arrival patterns and the same modes identified in the arrival patterns of the second inverse solution. And as can be seen in Figure 5.9, from about 350 meters to 500 meters, the ocean is still not modeled as well as it could be, but further mode group velocity inversions would solve that problem. The next logical step, however, is not further group velocity inversions, but a combined mode-ray inversion, which is out of the domain of this thesis.

The basic inversion scheme is to identify two or three of the lowest modes and then do a group velocity inversion to solve for the amplitudes of the first two EOFs. Using the inverse solution, it should now be possible to use the mode filter and identify the group velocities of several modes. Subsequent modal group velocity inversions should converge rapidly on a high-precision

model of the ocean. Rays may be included at any stage to extend the inversion to greater depths and to accelerate the convergence of the inversion procedure.

6. DISCUSSION AND CONCLUSIONS

The rapid means of calculating normal modes in a waveguide developed in seismology has been applied to ocean acoustics. This technique has allowed calculations that are more exact than traditional WKBJ and ray methods. Modal analysis can be used to answer a variety of questions concerning broad-band long-distance, deep-water sound propagation.

The most significant result concerns observing the onset of adiabicity in the top 500 meters of the Greenland Sea water column, in order to observe the formation of deep cold-water masses that affect the entire ocean's circulation. While WKBJ and ray theory are inadequate to monitor changes in this water acoustically at 250 Hz and 300 km range, normal mode theory is well suited to the task. Moreover, normal mode calulations of the acoustic arrival patterns in the top 500 meters can be faster than the WKBJ calculations.

For the first time, normal modes have been used to do tomographic inversions for sound speed. Quantifying the historical variation in the Greenland Sea with empirical orthogonal functions (EOFs) makes inversions based on modal group velocities converge

rapidly. Hybrid ray-mode inversions should achieve high precision, perhaps better than ±0.05 m/s or ±0.01^{0}C for the range-averaged ocean (although a true assessment of the achievable precision requires a formal resolution analysis, which is the subject of future work). Such extreme precision is particularly possible in the Greenland Sea because one of the primary sources of error in acoustic travel time measurements -- internal wave activity -- is apparently much smaller in the arctic than in the rest of the ocean [*Worcester, 1985*].

The mode filtering technique can enhance group velocity inversions by isolating individual modes through the use of acoustic waveforms observed at a variety of receiver depths. The mode filter requires multiple acoustic receivers set up as a vertical array. A 30 to 50 meter spacing with a relatively shallow (150 meter) source seems optimum. A shallow receiver close to 50 meters should allow the monitoring of Mode 0 during the winter, which would significantly improve the resolution of the top 100 meters of the ocean.

It does not appear that a smooth ice layer will have a significant effect on the propagation of sound in the Greenland Sea. Calculations suggest that only in regions of the ocean where the ice layer is of the order of 5 meters thick or more will sound propagation be significantly affected.

While WKBJ and ray theory are inadequate to describe sound propagation in the Greenland Sea, they are adequate prediction

techniques for typical range-independent mid-latitude profiles at 400 Hz with an axial source and receiver separated by a few hundred kilometers, as was found in the RTE83 experiment. For normal modes, the adiabatic approximation seems adequate to account for the effect of the range-dependence found in that experiment. This is the first experimental verification with high-precision data of what may be a more general conclusion -- that adiabatic normal mode theory may be adequate to handle a wide range of range-dependent sound speed fields [*Lynch, 1986* and *Desaubies, 1986*].

REFERENCES

Aki, K. and P. G. Richards, *Quantitative Seismology: Theory and Methods,* W. H. Freeman, San Francisco, California, 1980.

Boyles, C. A., *Acoustic Waveguides: Applications of Oceanic Science,* John Wiley and Sons, New York, 1984.

Brekhovskikh, L. M. and P. Lysanov, *Fundamentals of Ocean Acoustics,* Springer-Verlag, New York, 1982.

Brown, M.G., Application of the WKBJ Green's function to acoustic propagation in horizontally stratified oceans, *J. Acoust. Soc. Am., 71,* 1427-1432, 1982.

Chapman, C. H., The Earth flattening transformation in body wave theory, *Geophys. J. R. Astr. Soc., 35,* 55-70, 1973.

Desaubies, Y., A uniformly valid solution for acoustic normal mode propagation in a range varying ocean, *J. Acoust. Soc. Am., 76,* 524-626, 1984.

Desaubies, Y., C. Chiu, and J. Miller, Acoustic Mode Propagation in a Range Dependent Ocean (in preparation), 1985.

Desaubies, Y., WHOI/MIT, personal communication, 1986.

Ewing, M. W., W. S. Jardetzky, and F. Press, *Elastic Waves in Layered Media,* McGraw-Hill, New York, 1957.

Felsen, L. B., Hybrid ray-mode fields in inhomogeneous waveguides and ducts, *J. Acoust. Soc. Am., 69,* 352-361, 1981.

Gilbert, F., Ranking and winnowing gross Earth data for inversion and resolution, *Geophys. J. R. Astr. Soc., 23,* 125-128, 1971.

Gilbert, F. and G. Backus, *Geophysics, 31,* 326, 1966.

Haskell, N. A., The dispersion of surface waves in multilayered media, *Bull. Seismol. Soc. Amer., 43,* 17-24, 1953.

Howe, B., Ocean Acoustic Tomography: Mesoscale Velocities, Ph.D. Thesis, SIO/UCSD, 1986.

Lynch, J., MIT, personnal communications, 1986.

Masters, G., SIO, personnal communications, 1986.

Metzger, K. Jr., Signal processing equipment and techniques for use in measuring ocean acoustic multipath structures, Ph.D. Thesis, University of Michigan, Ann Arbor, 1983.

Milder, D. M., Ray and wave invariants for SOFAR channel propagation, *J. Acoust. Soc. Am., 46,* 1259-1263, 1969.

Muller, G., Exact ray theory and its application to the reflection of elastic waves from vertically inhomogeneous media, *Geophys. J. R. Astr. Soc., 21,* 261-283, 1970.

Munk, W. H. and C. Wunsch, Ocean acoustic tomography: a scheme for large scale monitoring, *Deep-Sea Research, 26,* 123-161, 1979.

Munk, W. H. and C. Wunsch, Ocean acoustic tomography: rays and modes, *Reviews of Geoph. and Space Physics, 21,* 777-793, 1983.

Munk, W. H., Horizontal deflection of acoustic paths by mesoscale eddies, *J. Phys. Oceanogr., 10,* 596-604, 1980.

Nagl, A., H. Uberall, A. J. Haug and G. L. Zaruv, Adiabatic mode theory of underwater sound propagation in a range-dependent environment, *J. Acoust. Soc. Am., 63,* 739-744, 1978.

Parker, R. L., Understanding Inverse Theory, *Ann. Rev. Earth Planet. Sci., 5,* 35-64, 1977.

Pekeris, C. L., Theory of propagation of explosive sound in shallow water, *Geol. Soc. Am. Mem. No. 27,* 1-117, 1948.

Pierce, A. P., Extension of the method of normal modes to sound propagation in an almost-stratified medium, *J. Acoust. Soc. Am., 37,* 19-27, 1965.

Rodi, W., P. Glover, T. Li and S. Alexander, A fast, accurate method for computing group-velocity partial derivatives for Rayleigh and Love modes, *Bull. Seismol. Soc. Amer., 65,* 1105-1114, 1975.

Stein, P. J., Acoustic monopole in a floating ice plate, Ph.D. thesis, MIT, 1986.

Swift, J. H., The Arctic Waters, in *The Nordic Seas,* B. Hurdle, ed., Springer-Verlag, New York, 1986.

Swift, J., University of Washington, personal communications, 1986.

Takeuchi, H. and M. Saito, Seismic Surface Waves, in *Methods in Computational Physics, Vol. II,* Bolt, B. A., ed., New York, 217-294, 1972.

Thomson, W. T., Transmission of elastic waves through a stratified medium, *J. Appl. Phys., 21,* 89-93, 1950.

Topuz, E. and L. B. Felsen, Hybrid representation of long-range sound pulse propagation in an underwater surface duct, *J. Acoust. Soc. Am., 78,* 1746-1756, 1985.

Woodhouse, J. H., Efficient and stable methods for performing seismic calculations in stratified media, *Proceedings of the International School of Physics "Enrico Fermi" Course 78,* 127-151, 1980.

Worcester, P. F., SIO, personal communications, 1986.

Worcester, P. F., R. C. Spindel and B. M. Howe, Reciprocal acoustic transmissions: Instrumentation for mesoscale monitoring of ocean current, *IEEE, J. Ocean Engr., OE-10,* 123-137, 1985.

APPENDIX ONE

A.1 Computation of Group Velocity

The technique described in Section 2.2 allows rapid calculation of the eigenvalues and eigenvectors of normal modes in a horizontally stratified ocean. In this appendix, it will be shown that this technique can easily be extended to rapidly calculate the modal group velocity at each frequency point the phase velocity is calculated. The entire treatment in this appendix follows Masters [*1986*].

Recalling the notation $b_1=dP/dz$ and $b_2=\omega P$, the equations of motion can be written $\partial b_2/\partial z = \omega \cdot b_1$ and $\partial b_1/\partial z = \omega \cdot h(\alpha) \cdot b_2$ where $h(\alpha)=[1/c^2-1/\alpha^2]$ and c is the horizontal phase velocity and is the eigenvalue or desired root of the vertical wave equation (equation T.8 in Chapter Two). Now

$$\partial(b_1 \cdot b_2)/\partial z = b_2 \cdot \partial b_1/\partial z + b_1 \cdot \partial b_2/\partial z = \omega \cdot (b_1)^2 + \omega \cdot (b_2)^2 h(\alpha)$$

When this is integrated from 0 to infinity (which will be the limits of all the integrals in this appendix), the left side vanishes because b_2 is zero at $z=0$ and $z=\infty$ at a root, and the result is

$$\int \omega \cdot (b_1)^2 \cdot dz = -\int \omega \cdot (b_2)^2 \cdot h(\alpha) \cdot dz \quad \text{at a root}$$

Since the ocean is divided into homogeneous layers in this scheme, the quantities b_1, b_2, and $h(\alpha)$ are constants in the layer and these integrals can be computed simply by summing over all the layers (or all the layers in which the eigenfunctions are still substantial). These two integrals provide a check that an eigenfunction is correct, for their ratio should be very close to one.

Rewriting the integrals in terms of $\dot{P}=b_1$ and $P=b_2/\omega$ gives

$$\int \dot{P}^2 \cdot dz = \omega^2 \cdot \int P^2 \cdot (1/\alpha^2 - 1/c^2) \cdot dz \qquad \text{A.1}$$

which is Rayleigh's principle [*Munk and Wunsch, 1983*].

Using Rayleigh's principle, the calculation of the group velocity, $u=d\omega/dk$, where $\omega=\omega(k)$, may be reduced to a sum over layers. Consider an eigenfrequency $\omega(k)$ with eigenfunction P and $\dot{P}$. Perturbing k to $k+\delta k$ gives

$$\omega \Rightarrow \omega + \delta\omega$$
$$P \Rightarrow P + \delta P$$
$$\dot{P} \Rightarrow \dot{P} + \delta\dot{P}$$

Substituting into equation A.1 gives

$$\int(\dot{P}+\delta\dot{P})^2\cdot dz = (\omega+\delta\omega)^2\cdot\int[(P+\delta P)^2/\alpha^2]\cdot dz - \int(k+\delta k)^2\cdot(P+\delta P)^2\cdot dz$$

which becomes, to first order

$$k\delta k\int P^2\cdot dz = \omega\delta\omega\int(P^2/\alpha^2)\cdot dz - \int\dot{P}\delta\dot{P}\cdot dz + \omega^2\int P\delta P(1/\alpha^2-k^2/\omega^2)\cdot dz$$

According to Rayleigh's principle, equation A.1, the last two integrals cancel (to first order in the perturbation), so

$$\omega\delta\omega\int(P^2/\alpha^2)\cdot dz = k\delta k\int P^2\cdot dz$$

or $\omega\delta\omega I_1 = k\delta k I_3$

where $I_1 = \int(P^2/\alpha^2)\cdot dz = (1/\omega^2)\int[(b_2)^2/\alpha^2)\cdot dz$

and $I_3 = \int P^2\cdot dz = (1/\omega^2)\int(b_2)^2\cdot dz$

This means that $u = \delta\omega/\delta k = I_3/(c\cdot I_1)$.

This equation allows rapid computation of the group velocity as each root is calculated, and it is at least as accurate as calculating nearby phase velocity roots and numerically differencing them. The method described in this appendix may be extended with a numerical differencing scheme to calculate quantities useful to tomographic inversions, such as the group velocity kernels discussed in Section 2.5 [*Rodi et al, 1975*].

APPENDIX TWO

A.2 Computation of Sound Propagation in Ice

The subject of this appendix is the numerical computation of the propagation of Rayleigh waves in the ice. For this, four variables are needed:

Y_1 -- the vertical displacement, here $u(z)\exp[i\cdot(\omega t-kr)]$

Y_2 -- the tangential displacement, here $u(r)\exp[i\cdot(\omega t-kr)$

Y_3 -- the vertical stress, τ_{zz}, here $(\tau_{zz}/\omega)\cdot\exp[i\cdot(\omega t-kr)$

Y_4 -- the tangential stress, τ_{zr}, here $(\tau_{zr}/\omega)\cdot\exp[i\cdot(\omega t-kr)$

where τ_{zz} and τ_{zr} are components of the stress tensor, $\boldsymbol{\tau}$.

As in Section 2.3, the entire discussion in this appendix follows Takeuchi and Saito [*1972*] and Woodhouse [*1980*], although the variables of the latter are used here. (In the former, Y_2 and Y_3 are transposed, and the stresses are not divided by ω.) The equations of motion are

$$dY_1/dz = \omega p\cdot[1-2\mu/\sigma]\cdot Y_2 + (\omega/\sigma)\cdot Y_3$$
$$dY_2/dz = -\omega p\cdot Y_1 + (\omega/\mu)\cdot Y_4$$
$$dY_3/dz = -\omega\rho_1\cdot Y_1 + \omega p\cdot Y_4$$
$$dY_4/dz = \omega\cdot[-\rho_1+4\mu p^2(1-\mu/\sigma)]\cdot Y_2 - \omega p(1-2\mu/\sigma)\cdot Y_3$$

ρ_1 is the density

$\sigma=\lambda+2\mu$, where λ and μ are Lamé parameters (μ is the rigidity)

p is the inverse phase velocity, $p=1/c=k/\omega$

This system of equations may be rewritten in the form

$$\partial Y/\partial z = \omega \mathbf{A} Y$$

where Matrix **A** is:

$$A = \begin{bmatrix} 0 & p(1-2\mu/\sigma) & 1/\sigma & 0 \\ -1/c & 0 & 0 & 1/\mu \\ -\rho_1 & 0 & 0 & 1/c \\ 0 & -\rho_1+4\mu p^2(1-\mu/\sigma) & -p(1-2\mu/\sigma) & 0 \end{bmatrix}$$

To reduce this system of equations in the solid to their equivalent form in the water -- which has density ρ_0 and sound speed α -- set the rigidity μ, the tangential stress Y_4, and its depth derivative dY_4/dz, all to zero. For $\mu=0$, $\sigma=\lambda=\rho_0\alpha^2$. The last condition ($dY_4/dz=0$) gives $Y_2=-(p/\rho_0)Y_3$ and that, coupled with the other conditions, gives

$$dY_1/dz = -(\omega/\rho_0)\cdot(p^2-1/\alpha^2)\cdot Y_3$$
$$dY_3/dz = -\omega\rho_0 Y_1$$

The equations used for water in Section 2.2 are

$$db_1/dz = \omega\cdot(p^2-1/\alpha^2)\cdot b_2$$
$$db_2/dz = \omega\cdot b_1$$

The solid equations reduces to the acoustic equations if

$$b_1 = Y_1$$
$$b_2 = -Y_3/\rho_0$$

This change of variables is needed because the propagator in the liquid was derived directly from the wave equation, and the density of water was implicity taken as a constant, whereas the propagator in the solid was taken from Woodhouse [*1980*]. The derivation provided here is for the sake of those who might use

and perhaps modify the normal mode program in the future.

It is now possible to derive the actual vectors used by the program at the liquid-solid interface. The above change of variables immediately gives the first interface conditions:

$$Y_1(z=0) = b_1(z=0) = b_{10}$$
$$Y_3(z=0) = -\rho_0 \cdot b_2(z=0) = -\rho_0 \cdot b_{20}$$

(This is the same as continuity of vertical stress and displacement.)

The first starting vector for $\mathbf{Y}$, $\mathbf{Y}_1 = (Y_{11}, Y_{12}, Y_{13}, Y_{14})$, at the bottom of the ice is therefore $(b_{10}, 0, -\rho_0 \cdot b_{20}, 0)$. The second, $\mathbf{Y}_1 = (Y_{11}, Y_{12}, Y_{13}, Y_{14})$ may be taken as $(0, Q, 0, 0)$ to represent an arbitrary horizontal displacement, Q, of the ice over the water. These two vectors are propagated to the top of the ice using the equations of motion. A root or eigenvalue, $c_n=\omega/k_n$, for the nth normal mode solution of the matrix equations of motion is found (and the value of Q is determined) whenever the value of the determinant $Y_{13}Y_{24} - Y_{23}Y_{14} \equiv \Delta$ is zero at the ice-air interface. When a root is located, the eigenvector is found by propagating the solution at the top of the ice back through the ice and then through the water. The propagator matrix for the ice, $P(z_2,z_1)$, satisfying $\mathbf{Y}(z_2)=P(z_2,z_1)\cdot\mathbf{Y}(z_1)$ and $dP(z_2,z_1)/dz=\mathbf{A}(z_2)\cdot P(z_2,z_1)$ can be derived from the matricized equations of motion and is given in Woodhouse [*1980*].

It turns out that the evaluation of Δ is numerically unstable, but the ice-propagation process can be stabilized by using the method of minors [*Gilbert and Backus, 1966*]. The remainder of this appendix will be directed to a brief summary of this method, following Woodhouse [*1980*].

If the two Rayleigh vectors in the ice are written as before, the minor vector **m** may be defined as

$$\mathbf{m} = [\mathbf{Y}_1, \mathbf{Y}_2] \equiv \begin{bmatrix} Y_{11}Y_{22} - Y_{12}Y_{21} \\ Y_{11}Y_{13} - Y_{13}Y_{21} \\ Y_{11}Y_{24} - Y_{13}Y_{21} \\ Y_{12}Y_{23} - Y_{13}Y_{22} \\ Y_{12}Y_{24} - Y_{14}Y_{23} \\ Y_{13}Y_{24} - Y_{14}Y_{23} \end{bmatrix} = \begin{bmatrix} m_1 \\ m_2 \\ m_3 \\ m_4 \\ m_5 \\ m_6 \end{bmatrix}$$

The notation $[\mathbf{Y}_1, \mathbf{Y}_2]$ stands for the minor of the two vectors, $\mathbf{Y}_1$ and $\mathbf{Y}_2$, formed by taking the six different, non-zero combinations (minors) of each vector as given above.

It can be shown that $m_2 = -m_5$ and that the minor vector satisfies a set of 5 coupled first order ordinary differential equations similar to those given at the beginning of this appendix.

The propagator for the minor vector is easily derived from these equations [*Woodhouse, 1980*]. The earlier condition on the values $\mathbf{Y}_1$ and $\mathbf{Y}_2$ for an eigenvalue -- $Y_{13}Y_{24} - Y_{23}Y_{14} \equiv \Delta = 0$ at the ice-air interface -- is here $m_6 = 0$ at the ice-air interface. The computational isolation of the eigenvalues is stabilized by propagating the minor vector $\mathbf{m}$ through the ice, rather than propagating $\mathbf{Y}_1$ and $\mathbf{Y}_2$ through the ice, since Δ is calculated directly. The initial value of $\mathbf{m}$ at the ice-water interface -- given before as initial values for the vectors $\mathbf{Y}_1$ and $\mathbf{Y}_2$ -- is now $(b_1, 0, 0, \rho_0 \cdot b_2, 0, 0)$. Further discussion of the minor vector propagator and the specific form of the integrals needed for determination of group velocity is given in Takeuchi and Saito [*1972*].